A Kinetic Theory for the Mechanics and Remodeling of Transient Anisotropic Networks

Franck J. Vernerey, Behnam Rezaei and Samuel Lamont
Department of Mechanical Engineering,
Program of Materials Science and Engineering,
University of Colorado, Boulder
USA

Abstract

We present a statistically-based theoretical framework to describe the mechanical response of dynamically crosslinked semi-flexible polymer networks undergoing finite deformation. The theory starts from a statistical description, via a distribution function, of the chain conformation and orientation. Assuming a so-called tangent affine deformation of the chains, this distribution is then allowed to evolve in time due to a combination of elastic network distortion and a permanent chain reconfiguration enabled by dynamic crosslinks. After presenting the evolution law for the chain distribution function, we reduce the theory to the evolution of the network conformation tensor in both its natural and current state. With this model, we use classical thermodynamics to determine how the stored elastic energy, energy dissipation, and true stress evolve in terms of the network conformation. We show that the model degenerates to classical anisotropic hyperelastic models when crosslinks are permanent, while we recover the classical form of the transient network theory (that describes hyper-viscoelasticity) when chains are fully flexible. Theoretical predictions are then illustrated and compared to the literature for both basic model problems and biomechanically relevant situations.

1. Introduction

Fibrous networks constitute the majority of soft connective tissues and bio-materials used in tissue engineering and bio-printing. They possess unique biochemical and mechanical properties for cells to proliferate, organize, and grow new tissues over time. Most of these biological fibrous tissues are made of semi-flexible filaments, whose contour length is on the order of (or smaller than) their persistence length. These types of networks are found in various forms and across several length scales. For instance, intermediate filaments and microtubules make up the major mechanical components of the cytoskeleton, while spectrin filaments provide the structural basis of the cortical membrane in red blood cells. Similarly, cellulose is the key building block of the cell walls of plants, fibrin networks ensure the mechanical integrity of blood clots, while collagen and elastin are responsible for extra-cellular matrix strength and flexibility [29]. The characteristic nonlinear elastic response of these networks has been the object of many studies from both theoretical and experimental sides. These models couple fiber realignment and the associated stress-stiffening, often defined by the J-shaped stress-strain curve [27]. Beyond their elastic response, biological networks are also known for their irreversible long-term reorganization, which plays an important role in both the reorganization of the cell cytoskeleton by molecular motors [6] and tissue remodeling by cells. One of the most striking examples of such rearrangements is the cell-induced long-range filament realignment and densification in collagen gels [29] [11].

¹correspondence to: franck.vernerey@colorado.edu

Inelastic filament rearrangement, which includes alignments with strains, reorientation, and bundling, is the result of relative and permanent motion at crosslinking points [24]. In most biological networks, this is mediated by dynamic crosslinkers 5 consisting of proteins of various sizes that can transiently bind to the filaments. While a single crosslinker is characterized by its average bond lifetime τ , the cumulative binding and unbinding events at the network level allow the material to behave elastically at time scales smaller than τ and visco-elastically at larger times. The viscoelastic and stress relaxation signature is not trivial as it usually possesses multiple relaxation times 28 and is associated with changes in the network's anisotropy. So how does a primarily elastic population of semi-flexible filaments, connected by elastic but transient bonds, yield a visco-plastic collective behavior? To answer this question, phenomenological anisotropic elastoplasticity models based on the multiplicative decomposition of the deformation gradient into an elastic and a plastic component have been widely utilized ([22, 12]). These models have been particularly useful in describing the filament rearrangement, stress-relaxation, and plastic deformation observed in fiber-reinforced composites and tissues where both matrix and fibers are inelastic. Microstructurally motivated models have also been developed to capture the temporal evolution of fibrous tissues using the statistical distribution of fibers as an internal variable \(\frac{19}{2} \). Although they provide a versatile tool to account for various types of fiber rearrangement, both at the matrix level and in the cytoskeleton 7 32, these models are still phenomenological. When it comes to the mechanics of dynamic networks, a deeper connection can be made between bond dynamics, chain elasticity, and the emerging network response. For instance, Green and Tobolsky [II] showed that the perpetual exchange of network connections must result in families of crosslinkers and filaments with different reference configurations. Based on this idea, continuum models were developed to account for chains being born at different times during loading, thereby possessing different relaxed configurations [15]. With the same idea but following a different point of view [14], the transient network theory (TNT) uses a statistical mechanics approach to follow the chain probability function over time as chains are simultaneously being convected with macroscopic deformation and undergoing bond exchange [35] 300. Both classes of theories have been able to successfully describe the complex behavior of various dynamic polymers, but are mostly limited to flexible networks with isotropic properties.

A generalization of the TNT to semi-flexible networks is not trivial since it must account for the change in configurations of two types of molecular objects: the filaments and the crosslinkers (as opposed to one chain population for flexible networks). Sridhar and Vernerey 26 showed that the structure of such a model should depend on the ratio R of the filament length to the crosslinker's length. When the flexible crosslinkers are long compared to the filaments (R < 1), the former dominates and the network response is captured by the TNT (i.e. filament alignment remains insignificant to the response due to their small size). When the filaments are on the order of the crosslinkers' size $(R \approx 1)$, several non-trivial nonlinear effects arise from the mechanical coupling between filaments' rotation and crosslinkers' stretch. Theoretically, a first model was introduced by Sridhar and Vernerey 26 to understand the mechanics of transient nematic networks, for which rods are strongly aligned and are assumed to rotate with the surrounding continuum. More recently, this approach was generalized to capture independent rod rotation and the associated effects including soft elasticity and the strain stiffening from rod realignment 31. Finally, when filaments are significantly longer than the flexible crosslinkers (i.e., R > 1), one should expect the response to be dominated by the filaments' elasticity and realignment. In this situation, the role of dynamic crosslinkers would mostly consist of relaxing the mechanical constraints between adjacent filaments over time. Thus, in this case, the theory can be based on the evolution of the configuration (stretch and orientation) of the filaments without considering the configuration of crosslinkers (which are too small to contribute significant elastic energy). In other words, the case of long filaments should result in a simplified, anisotropic version of the TNT. What's more, the case R > 1 is of particular importance for a variety of bio-polymers such as actin networks crosslinked by filamin, spectrin and other proteins in the cytoskeleton of most mammalian cells [25] 37]. The derivation of such a theory is the object of the present work.

The manuscript is organized as follows. In the next section, we introduce macroscopic descriptors of the (anisotropic) filament distribution through the statistical distribution ϕ of the filament's end-to-end vector and its associated covariance, denoted as the network conformation tensor. In the absence of bond dynamics,

this measure allows us to assess the network's elastic energy density under applied deformation. In section 3, we consider the case of dynamic crosslinkers to derive an evolution law for the natural and current filament distribution (and particularly their associated conformation tensors) as the network experiences macroscopic deformation. In section 4, we introduce constitutive relations for both the elastic response and the bond dynamics of these networks. Using thermodynamic principles, this naturally yields an expression for the elastic energy release rate and the stress tensor exhibited by these networks. In section 5, we finally explore the model predictions for a network under different modes of deformation. We also provide a comparison of the model with experimental data regarding the remodeling, relaxation, and self-healing of collagen gels. We find that the model can accurately capture the combined stress relaxation and network remodeling in a wide regime of strain and strain rates.

2. Mechanics of transient semi-flexible networks

In this section, our objective is to provide a macroscopic statistical description that is sufficient to describe the mechanical response of a semi-flexible network. These networks are made of filaments with a non-vanishing persistence length (i.e. they have a non-zero rest length) and that are crosslinked by molecules whose size is significantly smaller than the filament length. They could therefore exhibit preferred alignment, which can change over time due to either bonds being dynamic or depending on the deformation history. To characterize the elastic response of such systems, we first need to establish a mapping between the mean conformation of filaments in the current (or deformed) and a reference (or natural) state. For networks of flexible chains, this natural state is usually simple as it is represented by an isotropic distribution of chains with mean squared length $r_0^2 = Nb^2$. In contrast, a semi-flexible network does not possess a uniquely defined natural conformation since the chains, due to their non-vanishing rest length, may be organized in an anisotropic fashion. In the following, we describe the statistical framework to express these network conformations.

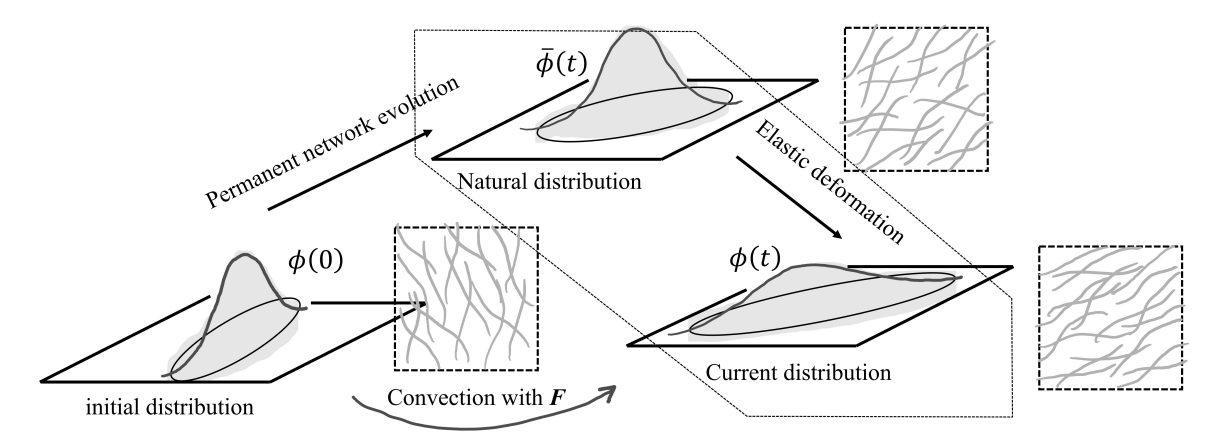


Figure 1: Relationships between the end-to-end distribution function during network deformation. The original network is defined by its initial distribution ϕ_0 that corresponds to a stress-free state. A macroscopic deformation gradient $\mathbf{F}(t)$ is then imposed on the network so that the distribution becomes ϕ in its current state, and $\bar{\phi}$ in its stress-free, natural state.

2.1. Probability distributions and macroscopic statistical descriptors

A starting point of the theory is a proper definition of the network statistics. For this, we describe the solid as a network of nodes connected by segments. The segments themselves may be described by their end-to-end vector \boldsymbol{r} (between two connections). It is convenient to decompose this vector as $\boldsymbol{r} = r\boldsymbol{u}$ where r is its length and \boldsymbol{u} is the unit vector indicating its direction. This direction can be expressed in a spherical coordinate system with inclination angle θ and the azimuth angle ϕ as:

$$\mathbf{u} = [\sin(\theta)\cos(\phi); \sin(\theta)\sin(\phi); \cos(\theta)] \tag{2.1}$$

The total number of segments (per unit reference volume) that can potentially be connected to the network is described by the nominal concentration c_t . Out of this population, the number of segments that are currently connected is referred to as c, while those that are disconnected (dangling ends) have a concentration $c_d = c_t - c$. To more accurately describe the conformation of connected chains, one can segregate segments depending on their conformation (or end-to-end vector). Doing so allows us to introduce the distribution of segment conformation as $\phi(\mathbf{r}) = cp(\mathbf{r})$, where p is the probability density indicating the likelihood of finding a connected segment in a given conformation \mathbf{r} . Such a probability density must verify the condition:

$$\int_{\Omega} p(\mathbf{r})d\Omega = 1 \tag{2.2}$$

where Ω designates the conformation space of segments, i.e. $r \in [0, \infty)$, $\theta \in [0, \pi]$ and $\phi \in [0, 2\pi)$. If there is no correlation between filament length and direction, the probability distribution can further be decomposed as:

$$p(\mathbf{r}) = q(r)s(\mathbf{u}) \tag{2.3}$$

where the probability densities q and s must verify:

$$\int_{r} q(r)r^{2}dr = 1 \quad \text{and} \quad \int_{\omega} s(\mathbf{u})d\omega = \int_{\theta=0}^{\pi} \int_{\phi=0}^{2\pi} s(\mathbf{u})sin\theta d\theta d\phi = 1$$
 (2.4)

Note that we used the short-hand notation ω to designate the solid angle, where $d\omega = \sin(\theta) dr d\theta d\phi$.

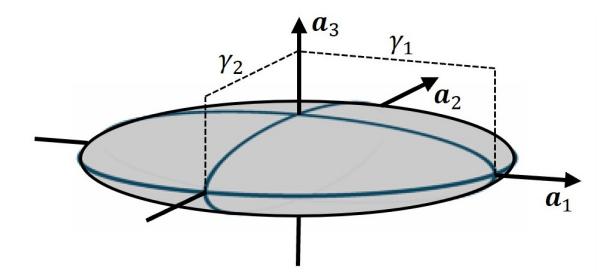


Figure 2: Graphical representation of the conformation tensor by an ellipsoid with principal axes along the $\{a_1, a_2, a_3\}$ directions. The length of each axis represents the variance of the filament distribution along each of these directions.

Although these distributions provide very detailed information about the network, they are usually cumbersome to work with. Thus, when possible, it is preferable to work with a reduced description, which can be done by only considering their covariances. The covariance tensor (sometimes referred to as the second central moment of the distribution) gives information about the spread of the distribution in different directions. It is a symmetric positive-definite tensor defined as:

$$\boldsymbol{\mu} = \frac{3}{r_0^2} \int_{\Omega} p(\boldsymbol{r}) \boldsymbol{r} \otimes \boldsymbol{r} d\Omega = \left[\frac{3}{r_0^2} \int_{r} q(r) r^2 dr \right] \left[\int_{\omega} s(\boldsymbol{u}) \boldsymbol{u} \otimes \boldsymbol{u} d\omega \right]$$
(2.5)

where we conveniently decomposed the integral over Ω (the conformation space) into an integral over length and another over the unit sphere. It is customary to normalize this covariance with respect to the quantity $r_0^2/3$ where r_0^2 represents the filament's mean square length in the reference conformation [35]. Each term in the above equation can be estimated as follows. The first term on the right-end side is a scalar quantity that measures the normalized mean filament length λ in the network, such that:

$$\lambda^2 = \frac{1}{r_0^2} \int_r q(r) r^2 dr \tag{2.6}$$

The second term on the right-end side of (2.5) is a tensorial quantity that describes the degree of filament anisotropy and mean direction. In the general case, it can be written:

$$h = \int_{\omega} s(\mathbf{u})\mathbf{u} \otimes \mathbf{u} d\omega = \gamma_1 \mathbf{a}_1 \otimes \mathbf{a}_1 + \gamma_2 \mathbf{a}_2 \otimes \mathbf{a}_2 + \gamma_3 \mathbf{a}_3 \otimes \mathbf{a}_3.$$
 (2.7)

where a_1 , a_2 and a_3 are three orthonormal vectors that point in the principal directions of the filament distribution, while the coefficient γ_1 , γ_2 , and γ_3 are three positive scalars that describe the shape of the distribution. In other words, the vectors a_i and coefficients γ_i are the eigenvectors and eigenvalues of the tensor h. It is therefore convenient to graphically represent this tensor by an ellipsoid as shown in Fig. where γ_1 , γ_2 , and γ_3 are the lengths of the principal axes. Note that since u is a unit vector, the trace of the above tensor must verify the condition $\gamma_1 + \gamma_2 + \gamma_3 = 1$. Therefore, writing $\gamma_3 = 1 - \gamma_1 - \gamma_2$ and using the fact that $I = a_1 \otimes a_1 + a_2 \otimes a_2 + a_3 \otimes a_3$, the tensor μ may be expressed in its principal frame as:

$$\mu = 3\lambda^{2} \left[(1 - \gamma_{1} - \gamma_{2}) \mathbf{I} + (2\gamma_{1} + \gamma_{2} - 1) \mathbf{a}_{1} \otimes \mathbf{a}_{1} + (2\gamma_{2} + \gamma_{1} - 1) \mathbf{a}_{2} \otimes \mathbf{a}_{2} \right]$$
(2.8)

The first component within the brackets represents the isotropic part of the filament distribution while the second and third constitute the (traceless) deviatoric part. In the remainder of this work, we refer to the tensor μ as the network conformation tensor. It can generally be defined in four states: (i) an initial (or reference) state, (ii) the current state, (iii) the natural state, and (iv) the reattachment state. We will introduce these in the following sections but also provide Table Π as a summary and reference for convenience.

Distribution	Description	Notation	\mathbf{CT}
Initial distribution	Probability distribution of segment vectors at an initial time t_0 . It is usually assumed to be at equilibrium	$p({m r},t_0)$	$\mu(0)$
Current distribution	Probability distribution of segment vectors at the current time t . This distribution does not necessarily correspond to an equilibrium state as segment filaments are usually in a deformed conformation	$p(m{r},t)$	$\mu(t)$
Natural distribution	Probability distribution of segment vectors in their relaxed conformation at the current time. This distribution corresponds to an equilibrium state and evolves over time due to bond association and dissociation and the resulting network rearrangement.	$ar{p}(m{r},t)$	$ar{m{\mu}}(t)$
Distribution at attachment	Probability distribution of segment vectors as they attach to the network. This distribution depends on the current network conformation.	$p_a({m r},t)$	$\mu_a(t)$

Table 1: Description of the probability distributions used in this work, and their notation. CT stands for conformation tensor.

2.2. Relaxed network conformation and stored elastic energy

The elastic energy stored in a network originates from the collective distortions of the filaments and crosslinks due to an imposed macroscopic deformation. Generally, when a network is subjected to deformation, the conformation of its filaments will be affected, such that the deformed conformation tensor potentially becomes distinct from its natural state. In this work, the natural state is described by its probability density \bar{p} , or equivalently, by the natural conformation tensor:

$$\bar{\boldsymbol{\mu}} = \frac{3}{r_0^2} \int_r \bar{p}(\boldsymbol{r}) \boldsymbol{r} \otimes \boldsymbol{r} d\Omega = 3\bar{\lambda}^2 \left[(1 - \bar{\gamma}_1 - \bar{\gamma}_2) \boldsymbol{I} + (2\bar{\gamma}_1 + \bar{\gamma}_2 - 1) \bar{\boldsymbol{a}}_1 \otimes \bar{\boldsymbol{a}}_1 + (2\bar{\gamma}_2 + \bar{\gamma}_1 - 1) \bar{\boldsymbol{a}}_2 \otimes \bar{\boldsymbol{a}}_2 \right] (2.9)$$

In its relaxed state, the network therefore has a mean square filament length $\bar{\lambda}^2$ and a degree of anisotropy provided by the quantities $\{\bar{\gamma}_1, \bar{\gamma}_2\}$ in principal directions $\{\bar{a}_1, \bar{a}_2\}$. Note that when filaments are elastic and crosslinks are permanent, the natural conformation tensor corresponds to the rotated initial (stress-free)

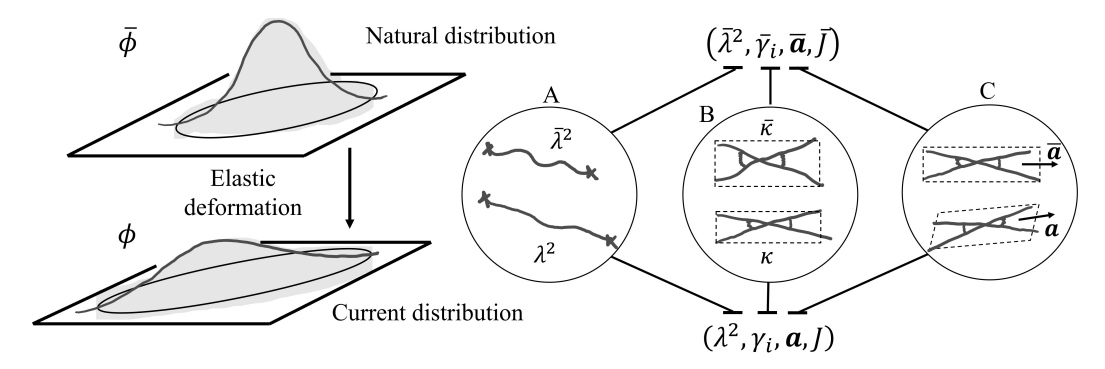


Figure 3: Network invariants in the natural and current conformation. The elastic energy stored in the network is a function of the difference in mean fiber stretch (A), the mean difference in network anisotropy (B), and the difference in the mean filament orientation (C), which is captured by the quantity $\cos \theta = \mathbf{a} \cdot \bar{\mathbf{a}}$. For clarity, the change in network anisotropy is shown at constant filament orientation, while the change in filament direction is shown at a constant degree of anisotropy. Both processes, which usually occur simultaneously, are related to a change in the average angle between filaments, as characterized by the invariant \mathscr{I}_2 introduced in equation (2.11). On the other hand, the difference in mean filament stretch is simply captured by the invariant \mathscr{I}_1 defined in equation (2.11)

network conformation $\bar{\mu} = R \cdot \mu(0) \cdot R^T$, where R is an orthogonal (rotation) tensor defined in equation (3.1). However, when crosslinks are dynamic, filaments may reorganize over time such that a relaxed network does not necessarily correspond to its initial state but rather evolves as a function of time and its strain history. Based on these definitions, the stored elastic energy can be estimated by comparing the natural and deformed network conformations. In this regard, we may define the difference tensor to be

$$\Delta \mu = \mu - \bar{\mu}.\tag{2.10}$$

We may further postulate that the mean elastic energy stored in the network filaments is a function of two invariants \mathscr{I}_1 and \mathscr{I}_2 . The first measures the difference in mean chain stretch:

$$\mathscr{I}_1 = \frac{1}{3}\Delta\boldsymbol{\mu} : \boldsymbol{I} = \lambda^2 - \bar{\lambda}^2 \tag{2.11}$$

The second measures the average difference in chain orientation:

$$\mathscr{I}_2 = \Delta \mu' : \Delta \mu' \quad \text{where} \quad \mu' = \frac{1}{3} \left[\frac{\mu}{\lambda^2} - I \right]$$
 (2.12)

is a deviatoric (traceless) measure of the conformation tensor μ . This quantity is independent of filament stretch and therefore only captures a change in the shape of the network conformation, which corresponds to changes in filament alignment and the degree of anisotropy. Taken together, the elastic energy density \mathscr{F} (measured per unit reference volume) can generally be written as:

$$\mathscr{F} = \mathscr{F}(c, \mathscr{I}_1, \mathscr{I}_2, J) \tag{2.13}$$

where \mathscr{F} is a continuous function of the arguments c, \mathscr{I}_1 , and \mathscr{I}_2 and the volumetric ratio $J = V/V_0$ with V and V_0 the deformed and initial volume of the network, respectively. We note that this energy functional arises from a statistical averaging of the locally stored energy in each single filament of the network [35]. Classical models for networks of semi-flexible filaments are discussed in section [4.3]

2.3. Special case of transversely isotropic networks

Although the ensuing presentation is for general three-dimensional networks, we here pay particular attention to transversely isotropic networks to better illustrate the physical meaning of the second invariant \mathscr{I}_2 . Transverse isotropy in the plane orthogonal to a_3 implies that $\gamma_1 = \gamma_2$ and the filaments partially align

(or misalign) along a single direction $a_3 = a$ in equation (2.8). The conformation tensor μ can then be written (the same formula applies to the relaxed conformation tensor $\bar{\mu}$):

$$\mu = \lambda^2 \left[\mathbf{I} + \kappa (3\mathbf{a} \otimes \mathbf{a} - \mathbf{I}) \right]$$
 where $\kappa = \frac{1}{2} \int_{\Omega} p(\mathbf{r}) (3\mathbf{u} \cdot \mathbf{a} - 1) d\Omega$ (2.14)

is the network degree of anisotropy (or order parameter [33]) that also verifies $\kappa = 1 - 3\gamma_1 = 1 - 3\gamma_2$. As depicted in Fig. [4], this order varies in the range $[-\frac{1}{2}, 1]$, where $\kappa = -\frac{1}{2}$ corresponds to a situation in which the filaments are isotropically distributed in a plane perpendicular to a, while $\kappa = 0$ corresponds to a fully isotropic network. On the other end of the spectrum, a positive κ indicates a preference for the filaments to align along a, with $\kappa = 1$ being associated with fully aligned filaments. The network conformation in its

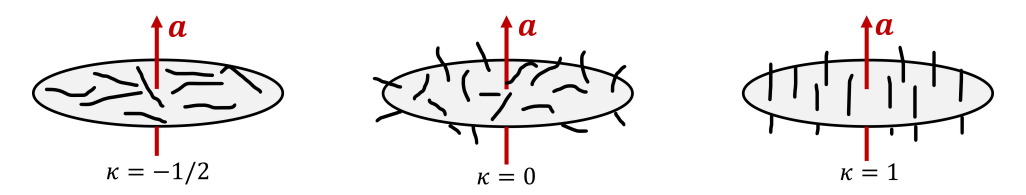


Figure 4: Illustration of the filament organization in a transversely isotropic network for particular values of the order parameter κ .

current and natural states can then be captured by three scalar quantities: the average stretch λ^2 , the order parameter κ , and the average misorientation $\cos \alpha = \boldsymbol{a} \cdot \bar{\boldsymbol{a}}$ between deformed and natural conformations. These quantities can be extracted from the conformation tensors as follows:

$$\kappa^2 = \frac{3}{2}\boldsymbol{\mu}' : \boldsymbol{\mu}' \qquad \bar{\kappa}^2 = \frac{3}{2}\bar{\boldsymbol{\mu}}' : \bar{\boldsymbol{\mu}}' \qquad \cos^2 \alpha = \frac{1}{3} + \frac{\boldsymbol{\mu}' : \bar{\boldsymbol{\mu}}'}{\kappa \bar{\kappa}}$$
 (2.15)

Furthermore, in this case, the second invariant (2.12) can be written in the form:

$$\mathscr{I}_2 = \frac{2}{3} \left[\left(\kappa - \bar{\kappa} \right)^2 + 3\kappa \bar{\kappa} \sin^2 \alpha \right] \tag{2.16}$$

We see here that \mathscr{I}_2 has two contributions: the first arises from a difference in the degree of anisotropy of a network between its current and natural state while the second simply arises from the average difference in chain orientation. The invariant vanishes identically when $\kappa = \bar{\kappa}$ and when the chain orientation is the same in both configurations (cos $\alpha = 1$).

3. Kinematics and network evolution

To describe the evolution of the network conformation with deformation, let us consider a macroscopic solid represented by the domains Ω_0 and Ω in its initial and deformed state, respectively. The mapping between these two domains is reflected by the motion $\boldsymbol{x} = \chi(\boldsymbol{X},t)$, where \boldsymbol{x} and \boldsymbol{X} are the coordinates of the same material point in the deformed and initial state and t is time. The deformation of the solid around the material point initially located in \boldsymbol{X} is then measured by the deformation gradient $\boldsymbol{F} = \partial \chi/\partial \boldsymbol{X}$. From this tensor, we can extract a pure rotation component \boldsymbol{R} and stretch component \boldsymbol{V} , such that:

$$\mathbf{F} = \mathbf{V} \cdot \mathbf{R} \tag{3.1}$$

Here, \mathbf{R} is an orthogonal tensor, while \mathbf{V} is the symmetric left stretch tensor. The rate of deformation can further be described by the velocity gradient ℓ such that $\ell = \dot{\mathbf{F}} \cdot \mathbf{F}^{-1}$, which consists of both a pure distortion and spin component. To connect the macroscopic deformation of the network with that of its constituents, we here use an affine assumption, where a connected filament temporally follows the macroscopic motion until it disconnects from the network via a random detachment event. In other words, we may assume that a

filament follows an affine deformation during its lifetime as a connected filament, i.e. between an attachment and a detachment event. This rule, which we call the *transient affine assumption*, can be expressed in rate form as 35:

$$\dot{\mathbf{r}} = \boldsymbol{\ell} \cdot \mathbf{r} \tag{3.2}$$

Note: The transient affine assumption only degenerates to the classical affine assumption $r = F \cdot r_0$ (where r_0 is the reference chain's end-to-end vector) for a permanently crosslinked network. Indeed, when crosslinks are dynamic, chains can dissociate and reassociate with the network several times during their lifetime, during which they reset their conformation. As a consequence, they do not follow an affine deformation in the classical sense.

3.1. Kinetic rates

Our main interest in this study is to understand the time-dependent response and evolution of a semi-flexible network when the crosslinking junctions between elastic filaments are dynamic. The word "dynamic" here refers to the case where junctions can temporally break and later reform between either different filaments or the same filaments, but possibly at different locations along their length. The way by which these events occur is stochastic and may be influenced by a variety of factors, such as chemistry, temperature, and mechanical forces. In this work, our objective is to consider perhaps the simplest situation, where these events occur at a mean frequency, denoted as k_a (for the rate of association) and k_d (for the rate of dissociation). The change in crosslinker density over time is then [35]:

$$\dot{c} = k_a(c_t - c) - k_d c \tag{3.3}$$

where we recall that c_t is the total concentration of crosslinkers and c only counts those that are connected to filaments at both of their ends. For convenience, let us define the bond exchange rate k as:

$$k = k_a \left(\frac{c_t}{c} - 1\right) = \frac{\dot{c}}{c} + k_d \tag{3.4}$$

This rate describes the speed at which new bonds are formed (and is normalized by the number of existing bonds). At equilibrium (i.e. when $\dot{c}=0$), we obtain $k=k_d$ and the rate at which bonds are created is exactly equal to the rate at which bonds dissociate. In the general situation, these rates may change during deformation. For instance, increasing fiber alignment may provide more opportunities for crosslinkers to bridge neighboring filaments, which would have the effect of raising the rate of attachment relative to the dissociation rate. Similarly, network damage is typically associated with a loss in crosslinking density [18] and a time-dependent bond exchange.

3.2. Evolution of the current network conformation

To determine how the network conformation evolves as a function of applied deformation and bond kinetics, we now need to present a differential equation for the distribution ϕ , whose evolution arises from the interplay between three physical processes: (a) the change in chain stretch that results from distorting the network at a rate set by the macroscopic velocity gradient ℓ , (b) the attachment of new filaments to the network with association rate k_a and occurring according to a distribution $p_a(r)$ and (c) the detachment of connected filaments in their stretched configuration with dissociation rate k_d . Based on these mechanisms, it can be shown that the distribution ϕ is the solution of the Fokker-Planck equation [35]:

$$\frac{D\phi}{Dt} = -\ell : \nabla(\phi \mathbf{r}) + k_a(c_t - c)p_a(\mathbf{r}) - k_d\phi(\mathbf{r})$$
(3.5)

where ∇ is the gradient operator with respect to the random variable \mathbf{r} . Recall that, as defined in table 1, the probability density function $p_a(\mathbf{r})$ represents the likelihood that an originally disconnected chain reconnects to the network with an end-to-end vector \mathbf{r} . For an incompressible network, $\operatorname{tr}(\boldsymbol{\ell}) \equiv 0$, and using

the decomposition $\phi(\mathbf{r}) = cp(\mathbf{r})$ as well as equations (3.4), the equation for the probability density becomes:

$$\frac{Dp}{Dt} = -\ell : (\nabla p \otimes r) + k (p_a - p)$$
(3.6)

where \otimes denotes the dyadic product. This evolution equation can be rewritten in terms of the conformation tensor μ defined in (2.5) by multiplying (3.6) by the tensor $r \otimes r$ and integrating over the chain conformation space. This eventually yields:

$$\frac{D\boldsymbol{\mu}}{Dt} = \boldsymbol{\ell} \cdot \boldsymbol{\mu} + \boldsymbol{\mu} \cdot \boldsymbol{\ell}^T + k\left(\boldsymbol{\mu}_a - \boldsymbol{\mu}\right)$$
(3.7)

Here, we introduced the conformation tensor μ_a of filaments during attachment events, expressed as:

$$\boldsymbol{\mu}_a = \frac{3}{r_0^2} \int p_a(\boldsymbol{r}) \boldsymbol{r} \otimes \boldsymbol{r} d\Omega \tag{3.8}$$

This tensor can usually be determined if one knows the average stretch and direction of filaments as they associate with the network. In general, we have little information on these molecular processes, and appropriate constitutive choices must be made as discussed in the next section. On an additional note, we recognize the lie derivative of the conformation tensor as convected by the deformation F as:

$$\mathscr{L}_{\ell}(\boldsymbol{\mu}) = \frac{D\boldsymbol{\mu}}{Dt} - \boldsymbol{\ell} \cdot \boldsymbol{\mu} - \boldsymbol{\mu} \cdot \boldsymbol{\ell}^T = \boldsymbol{F} \cdot \left[\frac{D}{Dt} \left(\boldsymbol{F}^{-1} \cdot \boldsymbol{\mu} \cdot \boldsymbol{F}^{-T} \right) \right] \cdot \boldsymbol{F}^T$$

This derivative may be interpreted as the change in network conformation relative to a frame that is convected with the velocity gradient ℓ . If the deformation is elastic (no bond dynamics), the network is simply convected with ℓ and this derivative vanishes, i.e. $\mathcal{L}(\mu) = 0$.

3.3. Evolution of the natural network conformation

The natural network conformation is not affected by elastic deformation, but rather by permanent changes in filament rearrangement. Thus, when no rearrangement takes place, the natural conformation is only convected by the rate of rotation $\Omega = \dot{R} \cdot \dot{R}^{-1}$. This ensures that objectivity requirements are verified. Furthermore, if the network undergoes the rearrangement discussed above, bond dissociation occurs in the current relaxed state $\bar{\phi}$ (i.e., elastically pulled back from the current distribution) while the reassociation occurs in the configuration p_a . The Fokker-Planck equation for the natural distribution is then:

$$\frac{D\bar{\phi}}{Dt} = -\mathbf{\Omega} : \nabla(\bar{\phi}\mathbf{r}) + k_a(c_t - c)p_a(\mathbf{r}) - k_d\bar{\phi}(\mathbf{r})$$
(3.9)

Again, using the decomposition $\bar{\phi} = c\bar{p}$, together with equations (3.4), we obtain an equation for \bar{p} of the form:

$$\frac{D\bar{p}}{Dt} = -\mathbf{\Omega} : (\nabla \bar{p} \otimes \mathbf{r}) + k (p_a - \bar{p})$$
(3.10)

This equation can now be rewritten in terms of the conformation tensor $\bar{\mu}$ defined in (2.5) using the same approach as above. This eventually yields:

$$\frac{D\bar{\boldsymbol{\mu}}}{Dt} = \boldsymbol{\Omega} \cdot \bar{\boldsymbol{\mu}} + \bar{\boldsymbol{\mu}} \cdot \boldsymbol{\Omega}^T + k\left(\boldsymbol{\mu}_a - \bar{\boldsymbol{\mu}}\right)$$
(3.11)

where we recognize here the objective Green-Naghdi rate $\mathscr{L}_{\Omega}(\bar{\mu})$.

$$\mathscr{L}_{\Omega}(\bar{\boldsymbol{\mu}}) = \boldsymbol{R} \cdot \left[\frac{D}{Dt} \left(\boldsymbol{R}^{-1} \cdot \boldsymbol{\mu} \cdot \boldsymbol{R}^{-T} \right) \right] \cdot \boldsymbol{R}^{T} = \frac{D\bar{\boldsymbol{\mu}}}{Dt} - \boldsymbol{\Omega} \cdot \bar{\boldsymbol{\mu}} - \bar{\boldsymbol{\mu}} \cdot \boldsymbol{\Omega}^{T}$$

Thus, without network reorganization (k=0), the natural conformation is only affected by rotation and $\mathcal{L}_{\Omega}(\bar{\mu}) = 0$. Equation (3.11) implies that the (rotated) natural network evolves towards a new configuration, given by the tensor μ_a .

4. Thermodynamically admissible constitutive relations

The time-dependent model can be summarized by the coupled evolution equations (3.7) and (3.11) for the current and natural conformation tensors with initial conditions $\mu(0) = \mu_0$ and $\bar{\mu}(0) = \bar{\mu}_0$. If the reference time is chosen such that the network is initially at equilibrium, we can further state that $\mu(0) = \bar{\mu}(0) = \mu_0$. These equations can be solved if two conditions are met: (i) the deformation history is known and specified through its time-dependent deformation gradient F(t) and (ii) the form of the conformation tensor μ_a is known at all times during the deformation history. As a consequence, two independent constitutive assumptions must be made to make predictions with this model. First, an explicit definition of a stored elastic energy density $\mathscr F$ as introduced in (2.13) must be proposed, and second an assumption for the mean attachment conformation tensor μ_a must be made. The former will be chosen to be consistent with previous work on the elasticity of such networks (see section (3.3)). The latter specifies the way by which a network reconfigures through the kinetic constant k. We begin by discussing this second quantity.

4.1. Attachment configuration

The conformation at which a population of filaments reconnect to the network could be quite complex and could depend on the environment, the nature of the filaments, and their history. Our goal here is to introduce the simplest possible model that is consistent with current observations regarding bond dynamics and remodeling [1, 36]. We then verify that this choice is consistent with the second principle of thermodynamics, i.e. that no energy is produced as a result of bond dynamics. Our constitutive assumptions can be summarized in three key points:

- First, a filament attaches in its natural, un-stretched length, which at the level of the population has a mean of r_0 . This implies that $\lambda_a^2 = 1$.
- Second, the current and attachment network conformations are characterized by the same overall filament orientation. This implies that the principal directions of the tensor μ_a are the same as the deformed conformation tensor μ .
- Third, filaments attach with a degree of anisotropy that is consistent with the network distribution at the time of attachment. Together with the previous assumption, this implies that $\mu'_a = \mu'$.

With these assumptions and using the expression for μ' defined in (2.12), the attachment configuration covariance tensor may be expressed in a simple form:

$$\mu_a = I + 3\mu' = \frac{\mu}{\lambda^2} \tag{4.1}$$

The finalized network evolution equations can be derived by substituting equation (4.1) into the general evolution equations (3.7) and (3.11). It is also convenient to use the decomposition $\bar{\mu} = \bar{\lambda}^2 (I + 3\bar{\mu}')$ to obtain the simple form:

$$\frac{D\boldsymbol{\mu}}{Dt} = \boldsymbol{\ell} \cdot \boldsymbol{\mu} + \boldsymbol{\mu} \cdot \boldsymbol{\ell}^T - k \left(\frac{\lambda^2 - 1}{\lambda^2}\right) \boldsymbol{\mu}$$
(4.2)

$$\frac{D\bar{\boldsymbol{\mu}}}{Dt} = \boldsymbol{\Omega} \cdot \bar{\boldsymbol{\mu}} + \bar{\boldsymbol{\mu}} \cdot \boldsymbol{\Omega}^T - 3k\left(\bar{\boldsymbol{\mu}}' - \boldsymbol{\mu}'\right)$$
(4.3)

Note that we used the trivial solution $\bar{\lambda}(t) = 1$ when the network starts at equilibrium, i.e., it is subjected to the initial condition $\bar{\lambda}(0) = 1$.

Let us now illustrate the consequences of these equations on filament stretch λ and alignment κ as follows. First, one can take the trace of the first equation to find the evolution of the mean square filament stretch as:

$$\frac{D\lambda^2}{Dt} = \frac{2}{3}\boldsymbol{\mu} : \boldsymbol{d} - k\left(\lambda^2 - 1\right) \tag{4.4}$$

We see here that the mean square stretch of the deformed network depends on two competing processes. First, a "convection" with the rate of deformation $\mathbf{d} = (1/2)(\ell + \ell^T)$, and second a relaxation from its current value λ to its value at attachment λ_a . This relaxation occurs at a characteristic time $1/k_d$, which coincides with the mean lifetime of a junction. To illustrate filament realignment, let us consider the special case of transversely isotropic networks for which the conformation tensors have the form (2.14). Substituting these forms in (4.3) and (4.2) yields evolution equation for the degrees of anisotropy κ and $\bar{\kappa}$:

$$\frac{D\kappa^2}{Dt} = 2(1 - \kappa)(1 + 2\kappa)\boldsymbol{\mu}' : \boldsymbol{d} \qquad \frac{D\bar{\kappa}^2}{Dt} = k\bar{\kappa} \left[2(\kappa - \bar{\kappa}) - 3\kappa \sin^2 \alpha \right]. \tag{4.5}$$

where α measures the filament angle between the current and natural configuration. The first equation implies that filament alignment in the deformed state directly follows from applied deformation and is independent of bond dynamics. Interestingly, the model predicts that the degree of filament alignment cannot change if either $\kappa=1$ (i.e. filaments are fully aligned with a) or $\kappa=-1/2$ (i.e. filaments are distributed in a plane orthogonal to a) as depicted in Fig. 4. Note that this is true if the network conformation is assumed to remain transversely isotropic under the rate of deformation rate a. The second equation further shows that the driving force for a permanent change in the degree of alignment linearly scales with the difference ($\kappa-\bar{\kappa}$) and the mean angle $\sin^2\alpha$ between the deformed and natural network conformations. Therefore, permanent realignment occurs at a rate of a0 until filament alignment coincides with the deformed and natural states.

4.2. Clausius-Duhem Inequality.

We now invoke the second law of thermodynamics, or alternatively, the Clausius-Duhem inequality, to determine the elastic energy release rate exhibited by the network as it reconfigures. This rate, expressed by the energy dissipation \mathcal{D} must remain positive at all times for the transformation to be admissible. For an isothermal process, dissipation can be written in the form:

$$\mathscr{D} = \boldsymbol{\sigma} : \boldsymbol{d} - \frac{\dot{\mathscr{F}}}{J} \ge 0 \tag{4.6}$$

where σ is the true stress tensor. For our energy density $\mathscr{F}(c, \mathscr{I}_1, \mathscr{I}_2, J)$, the material time derivative $\mathring{\mathscr{F}}$ is evaluated with the chain rule:

$$\dot{\mathcal{F}} = \frac{\partial \mathcal{F}}{\partial c}\dot{c} + \frac{\partial \mathcal{F}}{\partial \mathcal{I}_1}\dot{\mathcal{I}}_1 + \frac{\partial \mathcal{F}}{\partial \mathcal{I}_2}\dot{\mathcal{I}}_2 + \frac{\partial \mathcal{F}}{\partial J}\dot{J}. \tag{4.7}$$

After a lengthy calculation whose details are provided in appendix, we find that the change in free energy can be written in the convenient form:

$$\dot{\mathscr{F}} = \boldsymbol{\sigma} : \boldsymbol{d} - k \left[\mathscr{I}_1 \frac{\partial \mathscr{F}}{\partial \mathscr{I}_1} + 2 \mathscr{I}_2 \frac{\partial \mathscr{F}}{\partial \mathscr{I}_2} \right] + \frac{\partial \mathscr{F}}{\partial c} \dot{c}$$

$$(4.8)$$

where the Cauchy stress σ has the form:

$$\boldsymbol{\sigma} = \frac{2}{3J} \left[\frac{\partial \mathscr{F}}{\partial \mathscr{I}_1} \boldsymbol{\mu} + \frac{2}{\lambda^2} \frac{\partial \mathscr{F}}{\partial \mathscr{I}_2} \left((\boldsymbol{\mu}' - \bar{\boldsymbol{\mu}}') - ((\boldsymbol{\mu}' - \bar{\boldsymbol{\mu}}') : \boldsymbol{\mu}') \boldsymbol{I} \right) \cdot \boldsymbol{\mu} \right] + \frac{\partial \mathscr{F}}{\partial J} \boldsymbol{I}$$
(4.9)

Using equation (3.3) and substituting the result (4.8) into the dissipation (4.6) then yields:

$$\mathscr{D} = \frac{k_d}{J} \left(\mathscr{I}_1 \frac{\partial \mathscr{F}}{\partial \mathscr{I}_1} + 2 \mathscr{I}_2 \frac{\partial \mathscr{F}}{\partial \mathscr{I}_2} \right) + \frac{1}{J} \frac{\dot{c}}{c} \left[\left(\mathscr{I}_1 \frac{\partial \mathscr{F}}{\partial \mathscr{I}_1} + 2 \mathscr{I}_2 \frac{\partial \mathscr{F}}{\partial \mathscr{I}_2} \right) - c \frac{\partial \mathscr{F}}{\partial c} \right]$$
(4.10)

The condition $\mathscr{D} \geq 0$ imposes restrictions on the form of the constitutive equations. In particular, since k_d is a positive quantity, we choose the energy function \mathscr{F} such that the terms $\mathscr{I}_1 \frac{\partial \mathscr{F}}{\partial \mathscr{I}_1}$ and $\mathscr{I}_2 \frac{\partial \mathscr{F}}{\partial \mathscr{I}_2}$ always remain positive. Looking at the last term, another requirement of the second law is therefore:

$$\left[\left(\mathscr{I}_1 \frac{\partial \mathscr{F}}{\partial \mathscr{I}_1} + 2 \mathscr{I}_2 \frac{\partial \mathscr{F}}{\partial \mathscr{I}_2} \right) - c \frac{\partial \mathscr{F}}{\partial c} \right] \frac{\dot{c}}{c} \ge 0 \tag{4.11}$$

This condition enforces that no elastic energy can be provided to the system due to the association of new filaments into the network. If we consider equilibrated bond dynamics and thus $\dot{c} = 0$ at all times, this condition automatically satisfies the above requirement.

4.3. Stored elastic energy density

Consistent with our approach, the derivation of the network free energy should start at the level of a single chain by defining the energy $\psi(r)$ of a worm-like chain (WLC), where r is its end-to-end distance. The energy density of the network can then be estimated as:

$$\mathscr{F} = c \int_{\Omega} p(\mathbf{r})\psi(r)d\Omega \tag{4.12}$$

This approach is usually preferred as it connects the network mechanics to that of its fundamental constituents but may result in complicated constitutive equations. With this said our formulation can also be combined with simple empirical models. Thus, for the sake of simplicity, we here follow the approach presented by Gasser et al. \mathfrak{D} in choosing a strain energy that exponentially increases with the square of the first invariant \mathscr{I}_1 . We however enrich the model by adding an elastic contribution from filament reorientation through a linear dependency on \mathscr{I}_2 , leading to:

$$\mathscr{F}(\mathscr{I}_1, \mathscr{I}_2, J, c) = c \left[\frac{k_1}{2k_2} \left(\exp\left(k_2 \mathscr{I}_1^2\right) - 1 \right) + A \mathscr{I}_2 \right] + \frac{K}{2} \left(J - 1 \right)^2$$

$$\tag{4.13}$$

where k_1 , k_2 , and A are the material parameters and K can be interpreted as a bulk modulus that penalizes deviations of the volumetric stretch ratio $J = det(\mathbf{F})$ from unity. A major difference with the original model is the introduction of the term $A\mathscr{I}_2$ to account for the energy penalty associated with a change in chain orientation and the network's degree of anisotropy. The proposed energy function satisfies the thermodynamics restrictions stated earlier, i.e., a non-negative energy dissipation results from equation (4.10). Substituting (4.13) into equation (4.13), the Cauchy stress tensor is calculated as follows:

$$\boldsymbol{\sigma} = \frac{2c}{3J} \left[k_1 \mathscr{I}_1 \exp\left(k_2 \mathscr{I}_1^2\right) \boldsymbol{\mu} + \frac{2A}{\lambda^2} \left((\boldsymbol{\mu}' - \bar{\boldsymbol{\mu}}') - ((\boldsymbol{\mu}' - \bar{\boldsymbol{\mu}}') : \boldsymbol{\mu}') \boldsymbol{I} \right) \cdot \boldsymbol{\mu} \right] + K(J - 1) \boldsymbol{I}. \tag{4.14}$$

This is the form of the model used in the subsequent result section.

Note: Alternative models. While this is not the focus of the present work, we discuss here two alternative models for transversely isotropic networks, derived from the averaging operation (4.12) and based on the so-called mean field approximation. Both models can alternatively be used with the proposed approach, and yield results that are qualitatively similar to those presented in the next section. The first, proposed by Kuhl et al. [16] for transversely isotropic networks is based on the classical worm chain model and a repulsive term to account for the reference stress-free configuration. In this model, the average operation (4.12) is simplified by replacing the full network with eight representative chains located in a cubic unit cell of dimensions a, b, and b. The initial end-to-end length of the filament is then $r_0 = \sqrt{a^2 + 2b^2}/2$. The final form of the elastic potential is given by:

$$\mathscr{F} = \frac{ck_BT}{4l_p} \left[\left(2\frac{r^2}{L} + \frac{L^2}{L-r} - r \right) - \left(\frac{1}{L} + \frac{1}{4r_0[1 - \frac{r_0}{L}]^2} - \frac{1}{4r_0} \right) \left(\left(\frac{a^2 - b^2}{2} \right) \ln(I_4) + \frac{3b^2}{2} \ln(I_1^{(b)}) \right) \right]$$
(4.15)

where k_BT , l_p , and L are the thermal energy, the persistence length, and the contour length of the WLC, respectively. The quantity r is the average end-to-end length of the chains in the deformed configuration and can be calculated as (see appendix for details):

$$r = \frac{b\sqrt{3}}{2} \frac{\sqrt{\mathscr{I}_1 + 1}}{\sqrt{1 - \kappa_0}} \qquad \text{with} \qquad \kappa_0 = \frac{a^2 - b^2}{a^2 + 2b^2}. \tag{4.16}$$

The second model was introduced by Blundell and Terentjev [3] who introduced a slightly different model of the WLC chain, to account for its resistance to compressive forces. The associated energy function differs from earlier WLC formulations and is associated with a relaxed end-to-end distance where the filament experiences no stress. Although in the original paper, this energy is presented for a single chain, using a mean-field approximation based on the eight-chain unit cell, the strain energy for the network can be expressed in terms of the left Cauchy green tensor and its invariants to find:

$$\mathscr{F}(r) = ck_B T \left[\frac{\pi^2}{2} \frac{\ell_p}{L} \left(1 - \left(\frac{r}{L} \right)^2 \right) + \frac{2}{\pi} \frac{L}{\ell_p} \frac{1}{\left(1 - \left(\frac{r}{L} \right)^2 \right)} \right]$$

$$\tag{4.17}$$

where again, ℓ_p and L are the persistence and contour lengths of the filament, respectively, and r is defined in equation (4.16).

4.4. Discussion

Before exploring key predictions of the presented model, it is first useful to discuss its relationship to classical continuum models for the visco-plasticity and remodeling of filamentous networks. To begin, the presented model aligns with the transient network theory (TNT), which has predominantly been applied to flexible networks in the past (i.e., the persistence length of the filaments vanishes). The presented model thus represents a departure from the TNT introducing the effect of filament alignment and network anisotropy. A connection to the standard TNT can be made by considering flexible chains whose conformation at reattachment remains isotropic at all times since it is not affected by the surrounding network. The conformation of associating filaments in equation (4.1) must then be simplified by:

$$\mu_a = I \tag{4.18}$$

Substituting this expression into the evolution equation (3.7) quickly leads to the classical evolution equation presented in [35, 30]. Note that in this case, it is not necessary to keep track of a natural distribution as it remains isotropic at all times.

We now briefly discuss the differences and similarities of this approach with continuum models based on the multiplicative decomposition of the deformation gradient into elastic and inelastic contributions F_e and F_i , respectively:

$$\mathbf{F} = \mathbf{F}_e \cdot \mathbf{F}_i = (\mathbf{V}_e \cdot \mathbf{R}) \cdot \mathbf{U}_i = \mathbf{V}_e \cdot \mathbf{F}_i \tag{4.19}$$

where $F_i = R \cdot U_i$. This decomposition is based on the mapping of the deformation from an initial configuration \mathcal{B}_0 to an intermediate configuration \mathcal{B}_I by the tensor F_i , followed by the mapping from \mathcal{B}_I to the current configuration \mathcal{B} by the tensor F_e . Following standard practice in multiplicative decomposition in elasto-plasticity [20], rigid body rotation is included in the elastic deformation, such that $F_e = V_e \cdot R$ where V_e is the (symmetric) elastic left stretch tensor. As a consequence, the inelastic deformation leaves the intermediate configuration unrotated and can then be represented by the U_i . To be more consistent with the presented theory, the rotation may alternatively be incorporated into the inelastic contribution such that $F_i = R \cdot U_i$. A similar, yet different, type of decomposition was introduced for the network covariances in Fig. [1] It is therefore of interest to discuss the analogies between these two conceptual descriptions of the kinematics. To observe the difference between these two decompositions, first note that the classical approach is based on the affine convection of a small material element, which is undeformed in its initial state. Its final deformation is given by the mapping:

$$\boldsymbol{b} = \boldsymbol{F} \cdot \boldsymbol{I} \cdot \boldsymbol{F}^T \tag{4.20}$$

In contrast, the initial covariance of the network is not affinely convected with the deformation gradient. This is clear from equation (3.8) (when $k_a \neq 0$ and/or $k_d \neq 0$) which implies that the affine mapping is only a solution when the bond dynamics vanish. In general $\mu \neq F \cdot \mu_0 \cdot F^T$. Thus, the mapping between the

initial and current network conformation tensors is not described by the deformation gradient F. However, following the discussion in section 2, the mapping between the relaxed and current configuration is purely elastic and affine. Furthermore, since the intermediate frame rotates with the body, the elastic deformation only contains the stretch component V_e , such we can write:

$$\mu = V_e \cdot \bar{\mu} \cdot V_e \tag{4.21}$$

Multiplying each side of the equation by $\bar{\mu}$ from the right, the right stretch tensor may be determined by:

$$\mathbf{V}_e = (\sqrt{\boldsymbol{\mu} \cdot \bar{\boldsymbol{\mu}}}) \cdot \bar{\boldsymbol{\mu}}^{-1} \tag{4.22}$$

From the above arguments, it becomes clear that the inelastic deformation gradient F_i does not in general map the initial (μ_0) to the intermediate conformation tensor $(\bar{\mu})$. It may however be determined by the decomposition (4.19) as:

$$\mathbf{F}_i = \mathbf{V}_c^{-1} \cdot \mathbf{F} \tag{4.23}$$

Thus, when bond exchange does not occur $(k_d = 0)$, equation (4.2) implies that $\mu = \mathbf{F} \cdot \mu_0 \cdot \mathbf{F}^T$, while equation (4.3) yields $\bar{\mu} = \mathbf{R} \cdot \mu_0 \cdot \mathbf{R}^T$. Substituting the latter into (4.21) gives $\mu = \mathbf{F}_e \cdot \mu_0 \cdot \mathbf{F}_e^T$. Using the former, we find $\mathbf{F} = \mathbf{F}_e$. Therefore, in this situation, the inelastic deformation gradient becomes, from (4.23), $\mathbf{F}_i = \mathbf{R}$ (or $\mathbf{U}_i = \mathbf{I}$), i.e. the inelastic deformations vanish (which is expected for permanent cross-linking).

5. Results

We now illustrate the theory's predictions by considering the response of dynamic semi-flexible networks (characterized by their initial chain orientation and degree of anisotropy) in various loading conditions, which include the rate of loading and the loading history. In this context, evolution equations (4.2) and (4.3) imply that the change in conformation tensors depends on the competition between two timescales: the loading rate (described by $\tau_l = 1/|\ell|$) and the time of network reconfiguration (described by $\tau_n = 1/k$). Thus, rate effects may better be described by the non-dimensional Weissenberg number $W = \tau_n/\tau_l = |\ell|/k$ where $|\ell|$ is the spectral norm of the velocity gradient tensor ℓ . In the following, we first discuss the case of a large loading rate ($W \gg 1$) for which the materials response is essentially elastic. We then move to situations that are dominated by network rearrangement as observed during creep or stress-relaxation experiments. In all of the following sections, the value of the elastic parameter $k_2 = 1$, unless otherwise stated.

5.1. Elastic Response

The presented theory can predict the behavior of both elastic and dynamic networks. The elastic response can be considered either when the network consists of only covalent (permanent) crosslinkers or when the rate of deformation greatly exceeds the exchange rates exhibited by the crosslink dynamics. In these situations, the Weissenberg number $W \to \infty$ and the evolution equations degenerate to:

$$\frac{D\boldsymbol{\mu}}{Dt} = \boldsymbol{\ell} \cdot \boldsymbol{\mu} + \boldsymbol{\mu} \cdot \boldsymbol{\ell}^{T} \qquad \frac{D\bar{\boldsymbol{\mu}}}{Dt} = \boldsymbol{\Omega} \cdot \boldsymbol{\mu} - \boldsymbol{\mu} \cdot \boldsymbol{\Omega}$$
 (5.1)

The solution of these equations is given by the simple relations:

$$\mu = \mathbf{F} \cdot \mu_0 \cdot \mathbf{F}^T$$
 and $\bar{\mu} = \mathbf{R} \cdot \mu_0 \cdot \mathbf{R}^T$ (5.2)

This result implies that the natural conformation of an elastically deformed network can rotate. Using these equations, the invariants \mathscr{I}_1 and \mathscr{I}_2 may also be written in explicit form. Focusing on transversely isotropic networks, the mean square fiber stretch ratio λ^2 may be rewritten in terms of the deformation and the initial network order parameter κ_0 by substituting Equations (5.2) and (2.14) into (2.11), giving:

$$\mathscr{I}_1\left(I_1^{(b)}, I_4\right) = \frac{1}{3}(1 - \kappa_0)I_1^{(b)} + \kappa_0 I_4 - 1,\tag{5.3}$$

The second invariant of the conformation tensor \mathscr{I}_2 can also be written in terms of the invariants of the left Cauchy Green tensor (See appendix for the exact formula). Thus, we have $\mathscr{I}_1 = \mathscr{I}_1\left(I_1^{(b)},I_4\right)$ and $\mathscr{I}_2 = \mathscr{I}_2\left(I_1^{(b)},I_2,I_4,I_5\right)$, with the standard invariants $I_1^{(b)} = tr(\boldsymbol{b}), I_2 = \frac{1}{2}((tr(\boldsymbol{b}))^2 - tr(\boldsymbol{b}^2)), I_4 = \lambda_F^2$, and $I_5 = \boldsymbol{a_0} \cdot \boldsymbol{C}^2 \cdot \boldsymbol{a_0}$. The deformation and elastic energy of the network can therefore be described with five invariants: $I_1^{(b)}, I_2, I_4, I_5$, and J. The resulting Cauchy stress tensor may thus be expressed in the general form of an anisotropic hyperelasticity formulation (see, for example, [13]).

5.1.1. Fiber alignment induced strain stiffening

Let us now consider the effect of fiber alignment on the stiffening behavior of a semi-flexible network. Many of the biological semi-flexible networks used for *in-vitro* studies, such as type I collagen and fibrin gels, show strain stiffening, which is thought to arise from their fiber realignment [23] [4] [8]. These synthetic gels are commonly simple in makeup and may consist of only the desired filament crosslinked in a proper solvent. In contrast to synthetic gels, soft biological tissues, which also show strain-stiffening behavior, may be more complex and are often comprised of multiple networks 33. Thus, the strain-stiffening behavior exhibited by these systems may be dominated by different effects, such as the realignment of filaments and the stiffening of a single filament itself. In the present work, we explicitly account for the contribution of the fiber alignment through the term $A\mathscr{I}_2$ in the energy function (Eq. (4.13)). Meanwhile, the exponential term in Eq. (4.13)reflects the stiffening observed at the level of a single fiber as it is stretched to its contour length. The model may, thus, be most appropriate for a synthetic system that consists primarily of semi-flexible fibers. When considering a biological tissue, for instance, the energy of both the semi-flexible network and any secondary networks, which we may generally refer to as an isotropic "ground" matrix, must be considered. Historically, a neo-Hookean model has been used as an additional term in the free energy density to account for the ground matrixation. This was originally proposed by Gasser et al. to study the mechanics of arterial wall tissue \square . Thus, instead of including the term $A\mathscr{I}_2$ in Eq. (4.13), the neo-Hookean form $\frac{\mu_{sh}}{2}(I_1^{(b)}-3)$ may be added (where μ_{sh} is the shear modulus of the ground matrix). These two approaches are different in the way that they attribute the initial stiffness of the network as well as the subsequent strain-stiffening behavior.

To quantitatively explore the differences between these two classes of models, we compare their prediction for the tensile stress-strain response of initially isotropic networks. For the sake of comparison, the stretch-related coefficient k_2 is the same for both systems. In all cases, we apply an isochoric deformation with a maximum stretch of $F_{11} = 2$, where $F_{11} = e_1 \cdot F \cdot e_1$ and F is the deformation gradient in an orthonormal coordinate system described by the set of bases e_1, e_2, e_3 . In this case, a measure of uniaxial strain is provided by the scalar $\epsilon = F_{11} - 1$. Results are shown in Fig. 5 for both stress and stiffness $d\sigma/d\varepsilon$ for different values of A and μ_{sh} .

To promote the best comparison, for each value of A, we consider the value of the μ_{sh} that yields the same value of initial stiffness. Generally, increasing the coefficient of the alignment-related term A in our theory corresponds to initially stiffer networks. The same trend also stands for the model of Gasser et al. with a higher shear modulus μ_{sh} . Both stress σ and stiffness $d\sigma/d\varepsilon$ of the system increase with increasing the shear modulus of the NeoHookean model μ_{sh} and the coefficient of the alignment-related parameter A. The difference between the two models is not considerable for small network stretches. However, the differences in both stress and stiffness values become pronounced at larger values of the network strain. In contrast to the Neohookean model, the stiffness predicted by our model for different values of A converges to the same values as the network is stretched further. Note that in all cases, the fibers become oriented in the applied stretch direction ($\mathbf{a} = \mathbf{e}_1$) as the network is deformed (not illustrated).

Ignoring the Neo-Hookean embedding network in the Gasser model ($\mu_{sh} = 0$), results in a vanishing initial stiffness. Thus, our proposed energy formula allows us to model semi-flexible networks that are not necessarily embedded in other networks. However, the presented energy density function can be combined with other energy functions of other models. This allows us to model single semi-flexible networks, such as

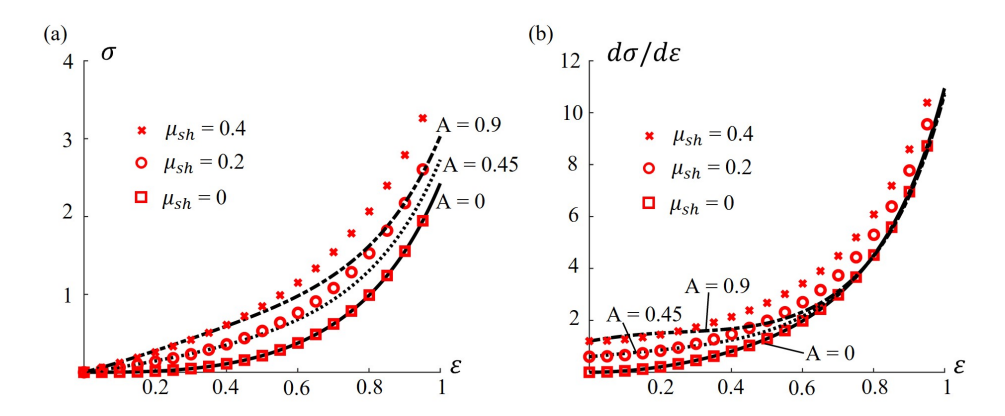


Figure 5: Comparison of the tensile response of an initially isotropic semi-flexible network using the model presented here (colored black) and the model presented by Gasser et al. \square . (colored red). The stress-strain curves (left) and the stiffness-strain curves (right) are plotted for A = 0, 0.45, 0.4 and $\mu_{sh} = 0, 0.2, 0.4$.

collagen gels, or semi-flexible networks that are combined with other soft networks, such as those found in the arterial wall. In the remainder of the examples, we consider a single semi-flexible network (i.e., $\mu_{sh} = 0$ and $A \neq 0$).

5.1.2. Realignment and reordering of fibers

To explore the effect of fiber alignment, we now simulate the response of an initially transversely isotropic network in uniaxial tension $(A/k_1 = 0.2)$. We consider two potential scenarios: First, the fibers are initially oriented along the direction of applied deformation. Second, the initial fiber orientation \mathbf{a}_0 is offset by an angle θ_0 to the applied loading. To promote better visualization, note that the alignment and degree of anisotropy of a network can be represented schematically by an ellipsoid (see Fig. 2). The three normal axes of the ellipsoid are in the principal directions of the conformation tensor \mathbf{a}_1 , \mathbf{a}_2 , and \mathbf{a}_3 , and their magnitudes are proportional to the eigenvalues of the conformation tensor γ_1 , γ_2 , and γ_3 , respectively. An isotropic network may then be illustrated by a sphere, while a transversely isotropic network is illustrated by an ellipsoid elongated in the direction of the main eigenvector (associated with the largest eigenvalue) of the conformation tensor and having two equal semi-axes. In Fig. 6 we plot the stress-strain curves and the change in order parameter κ (for the first scenario) and the direction of fibers α (for the second scenario) in the uniaxial tension experiment. In the first scenario, the network strain stiffens as filaments become more aligned with the stretch direction, as predicted by an increase in the parameter κ (Fig. 6a). Stress-strain curves and evolution of anisotropy κ are shown for three different values of the initial order parameter κ_0 .

Fig. 6b shows the stiffening behavior and filament realignment for three different values of fiber misalignment θ_0 , all of which have an initial order parameter $\kappa_0 = 0.25$. Note that $\theta_0 = 0$ corresponds to the case where filaments are aligned in the direction of the applied stretch. The study reveals that networks with a small initial misorientation θ_0 exhibit a stiffness that is primarily attributed to fiber stretch. This yields a comparatively stiff network response. By contrast, networks with a large initial misorientation exhibit a simultaneous change in fiber direction and stretching under applied force. This is illustrated by the curves showing fiber misorientation θ versus strain ε , where one can observe that filaments progressively realign and become more oriented in the same direction. The outcome of this realignment process is that misaligned networks appear much softer than their aligned counterpart.

Note: Although all networks started with transversely isotropic filament distribution, they no longer appear transversely isotropic after deformation. This can be seen by the ellipsoids shown in Fig. 6 which initially have two equal axes, as expected for a transversely isotropic network. However, as the network deforms, these axes do not remain equal $(\gamma_1 \neq \gamma_2 \neq \gamma_3)$ in equation (2.7), and the network becomes generally

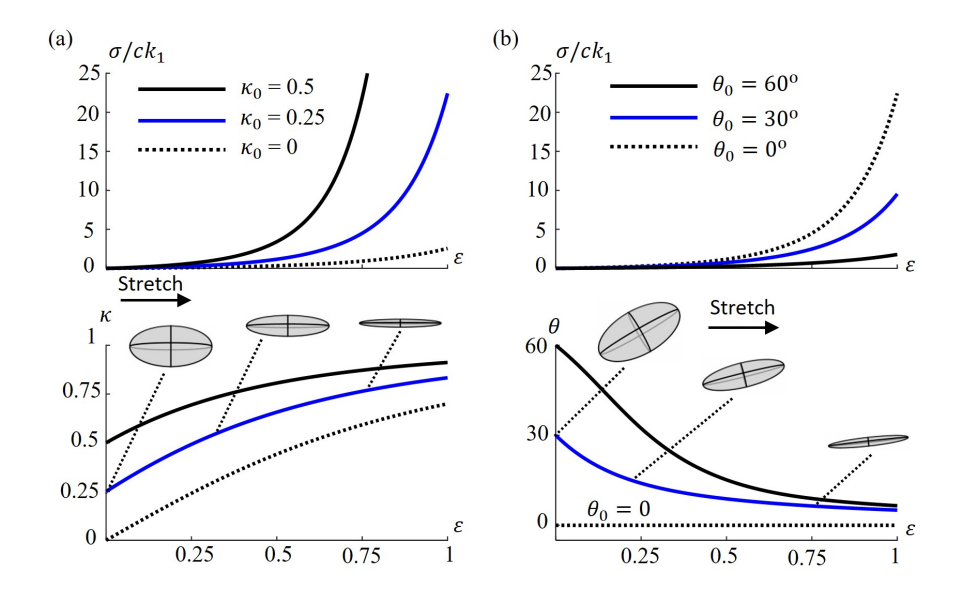


Figure 6: The tensile response of initially transversely isotropic network in a uniaxial tension test. a) The fibers are aligned with the fiber orientation. Stress-strain behavior and the evolution of the network degree of anisotropy $\bar{\kappa}$ are plotted for $\kappa_0 = 0, 0.25$, and 0.5. b) The fiber orientation is not aligned with the applied stretch. Stress-strain behavior and reorientation of the fibers $(\theta \text{ vs. } \varepsilon)$ are plotted for $\theta_0 = 0, 30$, and 60.

anisotropic.

5.2. Dynamic crosslinking and network remodeling

In dynamic networks, filament conformation can remodel over time and the mechanical behavior becomes dominated by bond dynamics. For simplicity, we here assume that the kinetic rates k_d and k_a remain constant over time. In this case, equation (3.3) is decoupled from deformation, and the density of attached filament c remains in a steady state condition ($\dot{c}=0$). This also implies that the exchange rate is now constant, with $k=k_d$ (from equation (3.4)) – a condition that fulfills the Clausius-Duhem inequality (4.10). In this section, the ratio of elastic parameters $A/k_1=0.2$ is taken to be constant.

5.2.1. Stress relaxation and remodeling

Most biological tissues and their bio-mimetic counterparts, which are composed of flexible and semi-flexible networks, exhibit a viscoelastic behavior. Creep and stress relaxation tests are usually performed to assess their mechanical characteristics. Here, we assess the model predictions regarding the behavior of a transversely isotropic network subjected to stress relaxation conditions (i.e., a quick uniaxial stretch $\varepsilon = 0.5$, followed by constant strain conditions). Again, two scenarios are explored, one where filaments are initially aligned with the stretch direction and another where they are initially misaligned by an initial angle θ_0 . Results regarding network evolution and the corresponding stress are summarized in Fig. [7]

For the first scenario, Fig. \bar{l}_{a} illustrates both the time evolution of stress and order parameter \bar{k} for three distinct initial order parameters. As previously observed, the model predicts that more ordered networks (large κ_{0}) are stiffer and thus exhibit larger stress for the same initial deformation. In the relaxation stage, the stress however follows an exponential decay curve dictated by the bond detachment rate k_{d} , independently of the initial network conformation. The origin of this relaxation can be traced back to the evolution of the natural configuration $\bar{\mu}$ over time. It is illustrated here with the change in order parameter $\bar{\kappa}$ of the natural configuration and by the graphical representations of the conformation tensors for the initial order parameter $\kappa(0) = 0.25$. Results indicate that the natural conformation does not change

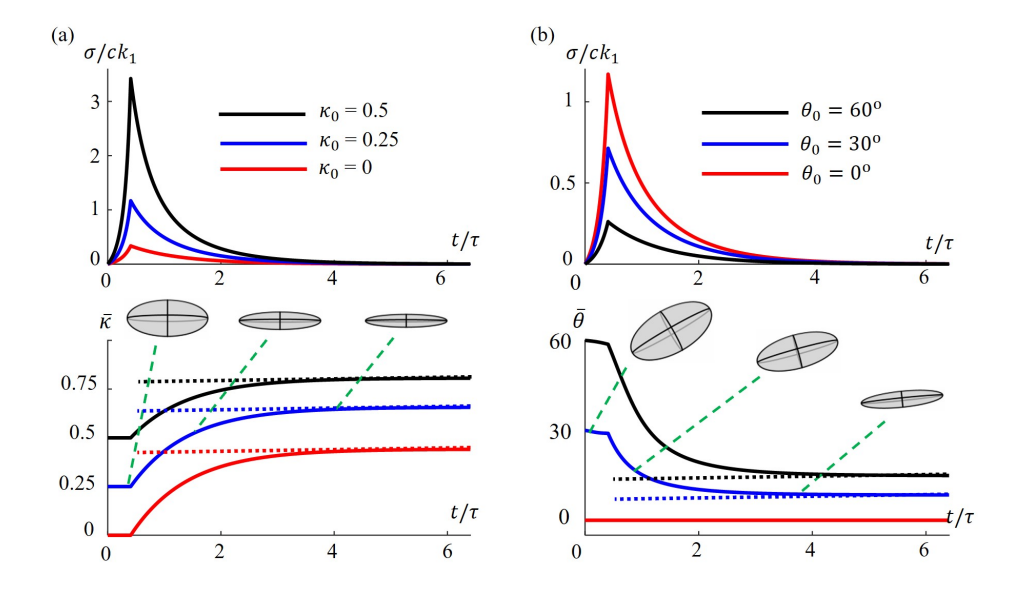


Figure 7: Unixial tension stress relaxation test for an initially transversely isotropic network. The network is stretched to $\varepsilon=0.5$ and then held indefinitely. a) Results when the fiber orientation is aligned with the applied stretch and for three different initial degrees of alignment. Stress vs. time and $\bar{\kappa}$ vs. time are plotted for $\kappa_0=0,0.25$, and 0.5. Dotted lines indicate the current value of κ which does not evolve during stress relaxation. b) Results for $\bar{\kappa}(0)=0.25$ and when the fiber orientation is not aligned with the applied stretch (the angle between them is θ_0). Stress vs. time and $\bar{\theta}$ vs. time are plotted for $\theta_0=0,30$, and 60. The evolution of the natural conformation tensor is visualized with the deformation of an ellipsoid, where the stretch direction is in the horizontal direction.

during fast elastic loading as $\bar{\kappa}$ remains constant since bond dynamics are much slower than the applied strain rate. However, during the relaxation stage, bond dynamics enable the natural network conformation to slowly evolve toward its current state (characterized by aligned filaments). At long times, the natural conformation eventually reaches a steady state, where filaments are permanently aligned with the stretched direction, indicating significant remodeling. The second scenario, whose results are shown in Fig. 7b (right) shows that stress relaxation of an anisotropic network arises from the reorientation of filaments that are initially misoriented with respect to the principal stretch direction. Consistent with the previous results, the model predicts a stiffer response when the filaments are initially oriented towards the axis of stretch. The relaxation stage is again characterized by an exponential stress decay at rate k_d . Once again, the relaxation process is related to the slow reorientation of the filaments in their natural state, which tends to relax their elastic energy over time. More specifically, we observe that while the (current) orientation of the filament does not change when the strain is held constant, their natural orientation evolves such that current and natural conformation become the same, at which point the stress vanishes. This can be readily observed in the initially misaligned networks $\theta_0 = 30^\circ$ and $\theta_0 = 60^\circ$ and is represented by the reorientation of the ellipsoid representing the network natural conformation tensor $\bar{\mu}$. On a final note, reorientation is not the only factor responsible for relaxation. Indeed, when the filaments are initially aligned with stretch ($\theta_0 = 0$), filaments remain in the same orientation during relaxation, but bond dynamics still result in energy release as they re-connect with the network at small strain. This results in a stress relaxation profile that is similar to other cases.

5.2.2. Permanent remodeling and elasticity recovery

The order parameter $\bar{\kappa}$ of the natural configuration can be considered a plastic realignment. It is not necessarily the same as the initial order parameter κ_0 and demonstrates the difference between the relaxed network and the initial network. To study the effect of relaxation time on the plastic realignment, we consider a relaxation-unloading test in which an initially isotropic network is elastically unloaded at specific times in

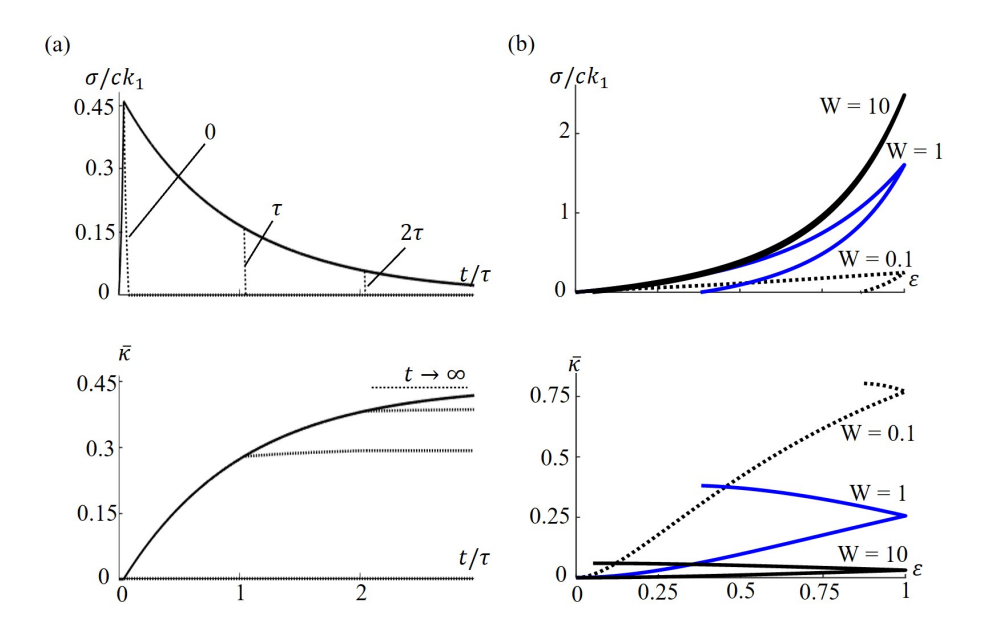


Figure 8: a) Relaxation unloading test for an initially isotropic network. The network is held for a predetermined holding time and then elastically unloaded to a state of zero stress. Top: Stress vs. time for holding times of $t_{hold} = 0$, τ , and 2τ where $\tau = 1/k_d$. Bottom: The evolution of \bar{k} for the same holding times b) The effect of Weissenberg number in a cyclic loading experiment on an initially isotropic network. Top) Stress-strain curve for W = 0.1, 10, and 10. Bottom) \bar{k} vs. strain for the same values of W.

the relaxation stage. Fig. Sa shows the evolution of stress σ/ck_1 for three different values of holding time (normalized by the relaxation time τ_n). It also depicts the evolution of the network's order parameter $\bar{\kappa}$ of its natural configuration for the same holding times. Together, these results show that as the network is held in a specific deformation state, its natural conformation slowly evolves towards the current state – a process that triggers the plastic realignment of filaments. As the network is elastically loaded during this process, the network can partially recover its initially stored elastic energy and conformation from connections that have not yet dissociated. From a theoretical perspective, this is described by the fact that the current state of alignment κ springs back to its natural value $\bar{\kappa}$. When this occurs, the current and natural conformations coincide and the network stress vanishes. This elastic recovery becomes less and less prominent over time since the natural alignment $\bar{\kappa}$ eventually converges to the current state at long times (Fig. Sa, bottom).

5.2.3. Rate effect (The Weissenberg Number)

The rate of loading determines the time provided for the dynamic bonds to reconfigure, and hence, affects the mechanical behavior of the network. To study the rate effect, we here simulate a cyclic loading test on an initially isotropic network that is first stretched to a predetermined strain and then elastically unloaded (to a stress-free state). Both loading and unloading paths take place at constant strain rates (or Weissenberg number $W = \dot{\epsilon}/k_d$), described by W = 10, 1, and 0.1. The stress-strain response and the evolution of the order parameter $\bar{\kappa}$ of the natural configuration are shown in Fig. 8 for all three conditions. The model predicts that for high strain rates, the unloading path is closer to the loading path since very little network reconformation takes place and the response remains quasi-elastic. However, as W decreases, the loading and unloading path difference becomes more pronounced, triggering a hysteresis loop that is characteristic of energy dissipation. This reflects the release of elastic energy from filament reconfiguration as bonds detach and re-associate. Fig. 8 also shows a significant increase of the order parameter $\bar{\kappa}$ (and therefore network remodeling) for small strain rates, while it remains relatively constant at high strain rates (W = 10). We finally note that for slow strain rates, the network does not return to its initial strain upon

unloading, indicating the presence of permanent deformation, in addition to plastic realignment.

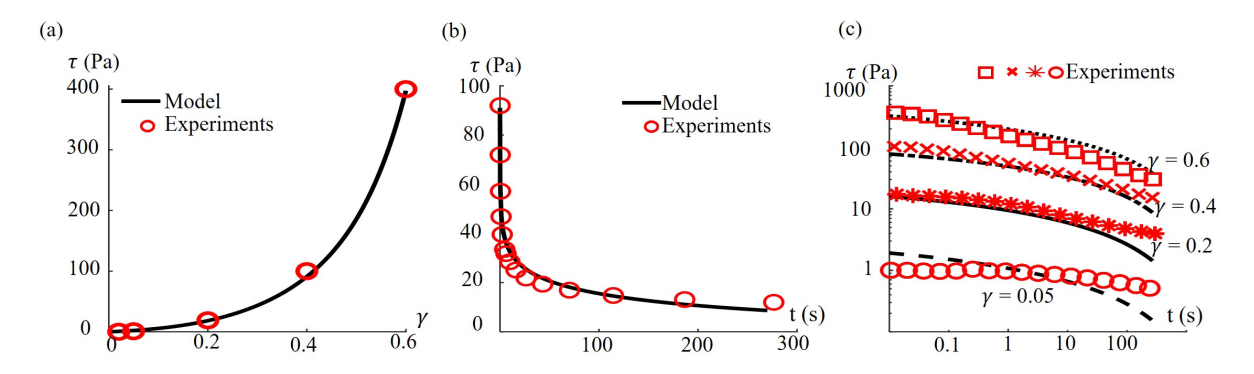


Figure 9: Experimental calibration of the presented model with the collagen gel data from Nam et al. [21] under shear loading a) Model prediction of the network maximum stress for different values of $\gamma = 0.4$. c) Stress prediction of the network with the parameters obtained for $\gamma = 0.4$ case for other values of shear strains

5.3. Force-dependent remodeling of collagen gels

To show the applicability of the presented model, we validate our results with published experimental data from Nam. et al. [21]. In this work, the authors performed stress relaxation tests on collagen gels for different values of constant shear strains γ . Using microscopy techniques, they also measured the distribution of the orientation of fibers before and after the relaxation test. Using these data, quantities can be compared with theoretical predictions. To do this, we first calibrate the proposed model using mechanical and structural data. More specifically, we use the experimentally observed distribution of fibers to calculate the initial conformation tensor $\mu(0)$. Furthermore, the shear stress-strain response of the gel in the elastic regime (under high strain rate), was used to determine elastic parameters to be $A=30~{\rm Pa\cdot m^3}$, $k_1=1430~{\rm Pa\cdot m^3}$, and $k_2=13.~{\rm Fig.}$ [9a shows the fitted shear stress-strain for these values.

The viscoelastic behavior of the collagen gel was then studied with stress relaxation. Upon attempting the calibrate the model with experimental data, we found that a model with a constant detachment rate k_d was not satisfactory. It is well-known that the rate at which bonds dissociate is affected by the applied mechanical force on the bonds, such that a large force yields a fast detachment rate. This type of response, characteristic of a *slip bond*, has been modeled with an exponential dependency of bond detachment rate with bond force, such as described by the Bell model 2 and others 1. To reproduce this effect at the continuum scale, we here propose a simplified law of the type:

$$k_d = k_d^0 \exp(\alpha \mathscr{F}). \tag{5.4}$$

where α is a parameter that characterizes the sensitivity of the mean detachment rate on the stored elastic energy and the base rate k_{d_0} describes bond dynamics in a stress-free state ($\mathscr{F} = 0$). In other words, the value of k_d approaches k_d^0 as the network relaxes. The values of k_d^0 and α were then calibrated using data describing the relaxation behavior for an applied constant strain $\gamma = 0.4$ as reported in [21]. A good agreement between theoretical predictions and data was found for $k_d^0 = 0.0015 \ 1/s$ and $\alpha = 0.06 \ 1/J$ as shown in Fig. [9]b. This result suggests that collagen gels indeed exhibit force-dependent bond dissociation. Using the calibrated values of k_{d_0} and α , we further proceeded to a validation exercise for relaxation experiments under different applied strains [21]. Fig. [9]c shows satisfactory results, confirming that the model properly captures the gel's nonlinear rheological behavior.

The process of bond reattachment in the network's stress-free state can be interpreted as a self-healing process. To illustrate this, Nam et al. performed two sequential stress-relaxation tests between which the

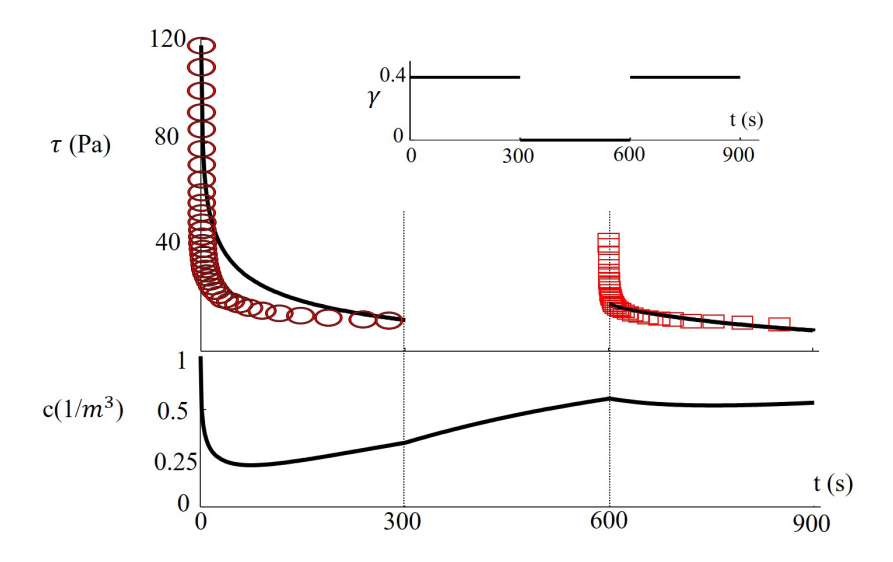


Figure 10: Two successive relaxation tests with a shear strain of $\gamma = 0.4$ where the network is allowed to equilibrate for 300s between the two tests. Self-healing predicted by our model in stress-time and chain density vs. time plots. Our model cannot fully capture the self-healing process from experiments

gel was allowed to equilibrate for 300 seconds (Fig. 10). Interestingly, experiments show that the gel recovers some of its elastic properties (stiffness) during the rest period since the initial stress in the second loading stage (at the same overall shear strain) is larger than the network stress at the end of the first relaxation stage. Simulating the same conditions with the model predicts a similar effect, albeit with a more dramatic stiffness recovery (A constant attachment rate $k_a = 0.5k_d^0$ was chosen in our simulations). To understand the cause of this self-healing process, Fig. [10] shows the evolution of the concentration of attached chains over time. The plot indicates that because the dissociation rate is a function of deformation, the chain concentration is not at equilibrium during mechanical loading. More specifically, the stretching phase of the test quickly increases the elastic energy stored in the filaments and as a consequence increases the rate of chain dissociation. This triggers a sharp decrease in the concentration of connected filaments as seen in the first few seconds. As the network relaxes, k_d reverts to its base value k_d^0 , prompting the chains to reconnect and the density c to slowly increase at a rate governed by the attachment rate. The model predicts that this self-healing dynamics extends to much after the first relaxation stage and within the rest period. As a result, the concentration c of connected filaments is larger at the start of the second relaxation stage than at the end of the first one. This explains the rise in stiffness owing to the linear relationship between concentration and stiffness (see equation (4.14)). A similar process was reported for flexible dynamic networks in a previous study 18.

6. Conclusion

In this study, we generalized the transient network theory to describe the time-dependent mechanical behaviors of anisotropic semi-flexible filaments featuring transient crosslinks. For this, we started by introducing macroscopic descriptors for the filament distribution, quantified by the statistical distribution ϕ of the filament's end-to-end vector and the associated conformation tensor. Subsequently, we formulated a Fokker-Planck equation that delineates the evolution of both natural and current filament conformation tensors under the influence of macroscopic deformation. This theoretical framework allows us to forecast the progressive evolution of filament configuration, the corresponding release of elastic energy, and the stress tensor over time. Notably, the presented model can accurately predict the combined phenomena of stress relaxation and network rearrangement across a broad spectrum of strain and strain rates. It also demonstrates predictive capabilities for network self-healing, making it a versatile approach to understanding and

predicting the mechanical responses of complex biological and bio-inspired networks with diverse structural characteristics.

This model serves as a foundation that can be expanded to encompass more intricate internal mechanisms. An example of such elaboration involves exploring the possibility that multiple bonds can potentially crosslink a single pair of semi-flexible filaments, such that they can collectively stabilize and reduce their overall detachment rate. Such a phenomenon may be an important factor to the process of filament bundling [29]. since aligned filaments geometrically increase opportunities for new bond association, which would induce a stabilizing effect. We therefore envision that the proposed model, in combination with discrete fiber simulation could be used to gain insights these intricate effects and the formation of filament bundles within semi-flexible networks. Furthermore, the current affine assumption remains a simplified approximation that could benefit from a more refined approach by conducting and analyzing the deformation in network-level simulations. This endeavor could for instance offer insights into the initiation and propagation of damage and fracture within the network and allow for a comprehensive examination of how these processes interact with the bond dynamics and self-healing mechanisms observed here. Finally, such a model could serve as a foundation for modeling active biological networks interconnected by molecular machines, such as myosin filaments in the actin cytoskeleton. By adapting this framework to capture the dynamic behaviors inherent to active networks, such models can pave the way for designing bio-inspired materials such as gels that use polyrotaxane slide-rings as crosslinks [34]. This class of application holds promise for creating bio-inspired materials with adaptive properties, drawing inspiration from the dynamic and self-regulating nature of biological networks.

7. Acknowledgment

FJV gratefully acknowledges the support of the National Science Foundation under Awards No. 2023179. The content is solely the responsibility of the authors and does not necessarily represent the official views of the National Science Foundation.

8. Appendix

8.1. Generalization of formulas for the 2D case

The presented statistical-based theory here can also be formulated for 2-dimensional networks. In the 2D case, some of the coefficients may differ from the 3D case. The main formulas of the 2D case are as follows:

• The covariance tensor:

$$\boldsymbol{\mu} = \frac{2}{r_0^2} \int_{\Omega} p(\boldsymbol{r}) \boldsymbol{r} \otimes \boldsymbol{r} d\Omega = \left[\frac{2}{r_0^2} \int_{\Omega} q(r) r^2 dr \right] \left[\int_{\omega} s(\boldsymbol{u}) \boldsymbol{u} \otimes \boldsymbol{u} d\omega \right]$$
(8.1)

• The invariants

$$\mathscr{I}_1 = \frac{1}{2}\Delta\boldsymbol{\mu} : \boldsymbol{I} = \lambda^2 - \bar{\lambda}^2 \tag{8.2}$$

$$\mathscr{I}_2 = \Delta \mu' : \Delta \mu' \quad \text{where} \quad \mu' = \frac{1}{2} \left[\frac{\mu}{\lambda^2} - I \right]$$
 (8.3)

• Special case of transversely isotropic network

$$\mu = \lambda^2 \left[I + \kappa (2a \otimes a - I) \right] \tag{8.4}$$

$$\lambda_I^2 = \frac{1}{2} \left[\boldsymbol{\mu}_I : \boldsymbol{I} \right] \qquad \kappa_I^2 = 2\boldsymbol{\mu}_I' : \boldsymbol{\mu}_I' \qquad \cos^2 \theta_{IJ} = \frac{1}{2} + \frac{\boldsymbol{\mu}_I' : \boldsymbol{\mu}_J'}{\kappa_I \kappa_J}$$
(8.5)

$$\mathscr{I}_1 = \frac{1}{2}\Delta\boldsymbol{\mu} : \boldsymbol{I} = \lambda^2 - \bar{\lambda}^2 \tag{8.6}$$

$$\mathscr{I}_2 = \frac{1}{2} \left[\left(\kappa - \bar{\kappa} \right)^2 + 4\kappa \bar{\kappa} \sin^2 \theta \right] \tag{8.7}$$

• Evolution of μ and $\bar{\mu}$:

$$\frac{D\boldsymbol{\mu}}{Dt} = \boldsymbol{\ell} \cdot \boldsymbol{\mu} + \boldsymbol{\mu} \cdot \boldsymbol{\ell}^T - k(\lambda^2 - 1) \left(\boldsymbol{I} + 2\boldsymbol{\mu}' \right)$$
(8.8)

$$\frac{D\bar{\boldsymbol{\mu}}}{Dt} = \boldsymbol{\Omega} \cdot \bar{\boldsymbol{\mu}} + \bar{\boldsymbol{\mu}} \cdot \boldsymbol{\Omega}^T - 2k\left(\bar{\boldsymbol{\mu}}' - \boldsymbol{\mu}'\right)$$
(8.9)

• The Cauchy stress tensor

$$\boldsymbol{\sigma} = \frac{2}{J} \left[\frac{\partial \mathscr{F}}{\partial \mathscr{I}_1} \boldsymbol{\mu} + \frac{1}{\lambda^2} \frac{\partial \mathscr{F}}{\partial \mathscr{I}_2} \left((\boldsymbol{\mu}' - \bar{\boldsymbol{\mu}}') - ((\boldsymbol{\mu}' - \bar{\boldsymbol{\mu}}') : \boldsymbol{\mu}') \boldsymbol{I} \right) \cdot \boldsymbol{\mu} \right] + \frac{\partial \mathscr{F}}{\partial J} \boldsymbol{I}, \tag{8.10}$$

8.2. Free energy time rate

Using the chain rule, the material time derivative of the free energy can be written as:

$$\dot{\mathscr{F}} = \frac{\partial \mathscr{F}}{\partial c}\dot{c} + \frac{\partial \mathscr{F}}{\partial \mathscr{I}_1}\dot{\mathscr{I}}_1 + \frac{\partial \mathscr{F}}{\partial \mathscr{I}_2}\dot{\mathscr{I}}_2 + \frac{\partial \mathscr{F}}{\partial J}\dot{J}. \tag{8.11}$$

Therefore, we need to calculate the time derivatives of the first and second invariants of the conformation tensor. For the first invariant, by combining Equations (2.11) and (4.4), we can write:

$$\dot{\mathscr{I}}_1 = \frac{D\lambda^2}{Dt} = \frac{2}{3}\boldsymbol{\mu} : \boldsymbol{d} - k\left(\lambda^2 - 1\right). \tag{8.12}$$

By expanding the right hand side of the Equation (2.12):

$$\mathscr{I}_2 = \mu' : \mu' + \bar{\mu}' : \bar{\mu}' - 2\mu' : \bar{\mu}', \tag{8.13}$$

hence

$$\dot{\mathscr{I}}_{2} = 2\dot{\mu}' : \mu' + 2\dot{\bar{\mu}}' : \bar{\mu}' - 2\dot{\mu}' : \bar{\mu}' - 2\dot{\bar{\mu}}' : \mu'$$
(8.14)

To calculate the time derivative of the traceless part of the conformation tensor, we use the evolution equation:

$$\boldsymbol{\mu} = \lambda^2 (\boldsymbol{I} + 3\boldsymbol{\mu}'), \tag{8.15}$$

By rearranging the above equation:

$$\dot{\boldsymbol{\mu}}' = \frac{1}{3\lambda^2} \left(\dot{\boldsymbol{\mu}} - \frac{D\lambda^2}{Dt} (\boldsymbol{I} + 3\boldsymbol{\mu}') \right)$$

$$= \frac{1}{3\lambda^2} \left(\boldsymbol{\ell} \boldsymbol{\mu} + \boldsymbol{\mu} \boldsymbol{\ell}^T + k(\boldsymbol{\mu}_a - \boldsymbol{\mu}) - \frac{D\lambda^2}{Dt} (\boldsymbol{I} + 3\boldsymbol{\mu}') \right)$$

$$= \frac{1}{3\lambda^2} \left(\boldsymbol{\ell} \boldsymbol{\mu} + \boldsymbol{\mu} \boldsymbol{\ell}^T + \left(-k(\lambda^2 - 1) - \frac{D\lambda^2}{Dt} \right) (\boldsymbol{I} + 3\boldsymbol{\mu}') \right)$$

$$= \frac{1}{3\lambda^2} \left(\boldsymbol{\ell} \boldsymbol{\mu} + \boldsymbol{\mu} \boldsymbol{\ell}^T - \left(\frac{2}{3} \boldsymbol{\mu} : \boldsymbol{d} \right) (\boldsymbol{I} + 3\boldsymbol{\mu}') \right)$$
(8.16)

Using the same approach:

$$\dot{\bar{\boldsymbol{\mu}}'} = \frac{1}{3}\dot{\bar{\boldsymbol{\mu}}} = \frac{1}{3}\left[\boldsymbol{\Omega}\cdot\bar{\boldsymbol{\mu}} + \bar{\boldsymbol{\mu}}\cdot\boldsymbol{\Omega}^T - 3k\left(\bar{\boldsymbol{\mu}}' - \boldsymbol{\mu}'\right)\right]. \tag{8.17}$$

We then, calculate all four terms in $\dot{\mathscr{I}}_2$

$$2\dot{\boldsymbol{\mu}}': \boldsymbol{\mu}' = \frac{2}{3\lambda^2} \left(\boldsymbol{\ell} \boldsymbol{\mu} + \boldsymbol{\mu} \boldsymbol{\ell}^T - \left(\frac{2}{3} \boldsymbol{\mu} : \boldsymbol{d} \right) (\boldsymbol{I} + 3\boldsymbol{\mu}') \right) : \boldsymbol{\mu}'$$

$$= \frac{2}{3\lambda^2} \left(\boldsymbol{\ell} \boldsymbol{\mu} + \boldsymbol{\mu} \boldsymbol{\ell}^T - \left(\frac{2}{3} \boldsymbol{\mu} : \boldsymbol{d} \right) (\boldsymbol{I} + 3\boldsymbol{\mu}') \right) : \frac{1}{3} \left(\frac{\boldsymbol{\mu}}{\lambda^2} - \boldsymbol{I} \right)$$

$$= \frac{2}{9\lambda^4} \left((\boldsymbol{\ell} \boldsymbol{\mu} + \boldsymbol{\mu} \boldsymbol{\ell}^T) : \boldsymbol{\mu} - \left(\frac{2}{3} \boldsymbol{\mu} : \boldsymbol{d} \right) \left(\frac{\boldsymbol{\mu}}{\lambda^2} \right) : \boldsymbol{\mu} \right) - 0$$

$$= \frac{2}{9\lambda^4} \left(2(\boldsymbol{\mu} \cdot \boldsymbol{\mu}) : \boldsymbol{\ell} - \frac{2\boldsymbol{\mu} : \boldsymbol{\mu}}{3\lambda^2} \boldsymbol{\mu} : \boldsymbol{\ell} \right)$$

$$= \frac{4}{9\lambda^4} \left(\boldsymbol{\mu} \cdot \boldsymbol{\mu} - \frac{\boldsymbol{\mu} : \boldsymbol{\mu}}{3\lambda^2} \boldsymbol{\mu} \right) : \boldsymbol{\ell},$$

$$(8.18)$$

where we used the identity:

$$(\boldsymbol{\ell}\boldsymbol{\mu} + \boldsymbol{\mu}\boldsymbol{\ell}^T) : \boldsymbol{\mu} = 2(\boldsymbol{\mu} \cdot \boldsymbol{\mu}) : \ell. \tag{8.19}$$

By doing the same procedure, the next three terms in the RHS of the Equation (8.14) can be written as:

$$2\dot{\bar{\boldsymbol{\mu}}}': \bar{\boldsymbol{\mu}}' = \frac{2}{3} \left[\boldsymbol{\Omega} \cdot \bar{\boldsymbol{\mu}} + \bar{\boldsymbol{\mu}} \cdot \boldsymbol{\Omega}^T - 3k \left(\bar{\boldsymbol{\mu}}' - \boldsymbol{\mu}' \right) \right] : \frac{1}{3} \left(\bar{\boldsymbol{\mu}} - \boldsymbol{I} \right)$$

$$= \frac{-2k}{3} (\bar{\boldsymbol{\mu}}': \bar{\boldsymbol{\mu}} - \boldsymbol{\mu}': \bar{\boldsymbol{\mu}}). \tag{8.20}$$

$$2\dot{\boldsymbol{\mu}}': \bar{\boldsymbol{\mu}}' = \frac{2}{3\lambda^2} \left(\boldsymbol{\ell} \boldsymbol{\mu} + \boldsymbol{\mu} \boldsymbol{\ell}^T - \left(\frac{2}{3} \boldsymbol{\mu} : \boldsymbol{d} \right) (\boldsymbol{I} + 3\boldsymbol{\mu}') \right) : \frac{1}{3} (\bar{\boldsymbol{\mu}} - \boldsymbol{I})$$

$$= \frac{2}{9\lambda^2} \left(2(\bar{\boldsymbol{\mu}} \cdot \boldsymbol{\mu}) : \ell - \frac{2\boldsymbol{\mu} : \bar{\boldsymbol{\mu}}}{3\lambda^2} \boldsymbol{\mu} : \ell \right)$$

$$= \frac{4}{9\lambda^2} \left(\bar{\boldsymbol{\mu}} \cdot \boldsymbol{\mu} - \frac{\boldsymbol{\mu} : \bar{\boldsymbol{\mu}}}{3\lambda^2} \boldsymbol{\mu} \right) : \ell.$$
(8.21)

$$2\dot{\bar{\boldsymbol{\mu}}}': \boldsymbol{\mu}' = \frac{2}{3} \left[\boldsymbol{\Omega} \cdot \bar{\boldsymbol{\mu}} + \bar{\boldsymbol{\mu}} \cdot \boldsymbol{\Omega}^T - 3k \left(\bar{\boldsymbol{\mu}}' - \boldsymbol{\mu}' \right) \right] : \frac{1}{3} \left(\frac{\boldsymbol{\mu}}{\lambda^2} - \boldsymbol{I} \right)$$

$$= \frac{-2k}{3\lambda^2} (\bar{\boldsymbol{\mu}}': \boldsymbol{\mu} - \boldsymbol{\mu}': \boldsymbol{\mu}). \tag{8.22}$$

Therefore, only two terms of \mathscr{I}_2 contribute to the Cauchy stress tensor, and the two other terms form the dissipation term. The Clausius-Duhem inequality (4.6) degenerates to:

$$\widetilde{\mathcal{G}} = \left[\sigma - \frac{1}{J} \left(\frac{\partial \mathscr{F}}{\partial \mathscr{I}_{1}} \left(\frac{2}{3} \mu \right) + \frac{\partial \mathscr{F}}{\partial \mathscr{I}_{2}} \left(\frac{4}{9\lambda^{4}} \left(\mu \cdot \mu - \frac{\mu : \mu}{3\lambda^{2}} \mu \right) - \frac{4}{9\lambda^{2}} \left(\bar{\mu} \cdot \mu - \frac{\mu : \bar{\mu}}{3\lambda^{2}} \mu \right) \right) + \frac{\partial \mathscr{F}}{\partial J} J \boldsymbol{I} \right) \right] : \ell \\
+ \frac{k}{J} \left(\frac{\partial \mathscr{F}}{\partial \mathscr{I}_{1}} (\lambda^{2} - 1) + \frac{2}{3} \frac{\partial \mathscr{F}}{\partial \mathscr{I}_{2}} \left(\bar{\mu}' : \bar{\mu} - \mu' : \bar{\mu} - \frac{\bar{\mu}' : \mu}{\lambda^{2}} + \frac{\mu' : \mu}{\lambda^{2}} \right) \right) - \frac{\dot{c}}{J} \frac{\partial \mathscr{F}}{\partial c} \ge 0$$

So, the Cauchy stress tensor is derived as:

$$\boldsymbol{\sigma} = \frac{2}{3J} \left[\frac{\partial \mathscr{F}}{\partial \mathscr{I}_1} \boldsymbol{\mu} + \frac{2}{3\lambda^2} \frac{\partial \mathscr{F}}{\partial \mathscr{I}_2} \left(\frac{\boldsymbol{\mu}}{\lambda^2} - \bar{\boldsymbol{\mu}} - \left(\frac{\boldsymbol{\mu} : \boldsymbol{\mu}}{3\lambda^4} - \frac{\boldsymbol{\mu} : \bar{\boldsymbol{\mu}}}{3\lambda^2} \right) \boldsymbol{I} \right) \cdot \boldsymbol{\mu} \right] + \frac{\partial \mathscr{F}}{\partial J} \boldsymbol{I}, \tag{8.24}$$

Further, using $k = k_d + \frac{\dot{c}}{c}$, $\mu = \lambda^2 (I + 3\mu')$, and $\bar{\mu} = I + 3\bar{\mu}'$ the dissipation terms degenerates to:

$$\mathscr{D} = \frac{k_d}{J} \left(\mathscr{I}_1 \frac{\partial \mathscr{F}}{\partial \mathscr{I}_1} + 2 \mathscr{I}_2 \frac{\partial \mathscr{F}}{\partial \mathscr{I}_2} \right) + \frac{1}{J} \frac{\dot{c}}{c} \left[\left(\mathscr{I}_1 \frac{\partial \mathscr{F}}{\partial \mathscr{I}_1} + 2 \mathscr{I}_2 \frac{\partial \mathscr{F}}{\partial \mathscr{I}_2} \right) - c \frac{\partial \mathscr{F}}{\partial c} \right]. \tag{8.25}$$

8.3. Expressing the second invariant in terms of the Left Cauchy Green Tensor Invariants

In the following equation, if we set $\lambda^2 = \frac{(1-\kappa_0)}{3}I^{(b)} + \kappa_0 I_4$, the final form of \mathscr{I}_2 is only a function of the left Cauchy tensor invariants.

$$\mathscr{I}_{2}\left(I_{1}^{(b)}, I_{2}, I_{4}, I_{5}\right) = \frac{(1-\kappa_{0})^{2}}{9} \left(\frac{I_{1}^{(b)^{2}} - 2I_{2}}{\lambda^{4}} - \frac{2I_{1}^{b}}{\lambda^{2}} + 3\right) + \kappa_{0} \left(\frac{I_{4}^{2}}{\lambda^{4}} - \frac{2I_{2}\cos^{2}\theta}{\lambda^{2}} + 1\right) + \frac{2\kappa_{0}(1-\kappa_{0})}{3} \left(\frac{I_{5} - 2I_{4} - 1}{\lambda^{2}} + 1\right), \tag{8.26}$$

8.4. Derivation of the stress for Blundell-Terentjev strain energy

As an illustration of the model, we follow the approach presented by Blundell and Trenjev [3] to present an energy function for transversely isotropic chain networks. For a single filament, taking advantage of the wormlike chain (WLC) model, one can derive the strain energy of the WLC filament as:

$$\psi_c(\hat{r}) = k_b T \left[\frac{\pi^2}{2} \frac{\ell_p}{L} \left(1 - \hat{r}^2 \right) + \frac{2}{\pi} \frac{L}{\ell_p} \frac{1}{(1 - \hat{r}^2)} \right], \tag{8.27}$$

where $\hat{r}=r/L$ is the normalized end-to-end distance of the chain. L, k_b, T , and l_p represent the filament contour length, the Boltzmann constant, absolute temperature, and the filament persistence length respectively. Based on this model, the semiflexible chain has an equilibrium end-to-end length of $r_{eq}=L(1-\frac{2k_bTL}{\pi^{(3/2)A}})^{1/2}$. Considering an eight-chain model, in which eight WLC chains of the same size are embedded inside a unit cell with initial dimensions of a, b, and b (a transversely isotropic unit cell), the initial anisotropy and the end-to-end distance of the deformed network is calculated as

$$\kappa_0 = \frac{a^2 - b^2}{a^2 + 2b^2}$$
 and $r = \frac{b\sqrt{3}}{2} \frac{\sqrt{\mathscr{I}_1 + 1}}{\sqrt{1 - \kappa_0}}$ (8.28)

The strain energy function is defined as follows:

$$\psi(\mathscr{I}_1, J) = k_1 \left[k_2 - k_3 \mathscr{I}_1 + \frac{\pi}{k_2 - k_3 \mathscr{I}_1} \right] + \frac{K}{2} (J - 1)^2$$
(8.29)

The constants k_1 , k_2 , and k_3 are related to the parameters of equation (8.27) as:

$$k_1 = cK_bT, (8.30)$$

$$k_2 = \frac{\pi^2 l_p}{2L} \left(1 - \frac{3b^2}{4L^2(1 - \kappa_0)} \right), \tag{8.31}$$

$$k_3 = \frac{\pi^2 l_p}{2L} \frac{3b^2}{4L^2(1-\kappa_0)} \tag{8.32}$$

The derivatives of the energy function, thus are as follows:

$$\frac{\partial \psi}{\partial \mathscr{I}_1} = -k_1 k_3 + \frac{\pi k_1 k_3}{(k_2 - k_3 \mathscr{I}_1)^2},\tag{8.33}$$

$$\frac{\partial \psi}{\partial J} = K(J-1). \tag{8.34}$$

Hence, the Cauchy stress for this model is

$$\boldsymbol{\sigma} = \frac{2k_1}{3J} \left[\left(-k_3 + \frac{\pi k_3}{(k_2 - k_3 \mathcal{I}_1)^2} \right) \boldsymbol{\mu} \right] + K (J - 1) \boldsymbol{I}$$
 (8.35)

References

- Ehsan Ban, J Matthew Franklin, Sungmin Nam, Lucas R Smith, Hailong Wang, Rebecca G Wells, Ovijit Chaudhuri, Jan T Liphardt, and Vivek B Shenoy. Mechanisms of plastic deformation in collagen networks induced by cellular forces. Biophysical journal, 114(2):450-461, 2018.
- [2] George I Bell. Models for the specific adhesion of cells to cells: a theoretical framework for adhesion mediated by reversible bonds between cell surface molecules. Science, 200(4342):618–627, 1978.
- [3] JR Blundell and EM Terentjev. Buckling of semiflexible filaments under compression. Soft Matter, 5(20):4015–4020, 2009.
- [4] André EX Brown, Rustem I Litvinov, Dennis E Discher, Prashant K Purohit, and John W Weisel. Multiscale mechanics of fibrin polymer: gel stretching with protein unfolding and loss of water. science, 325(5941):741–744, 2009.
- [5] Federica Burla, Yuval Mulla, Bart E Vos, Anders Aufderhorst-Roberts, and Gijsje H Koenderink. From mechanical resilience to active material properties in biopolymer networks. *Nature Reviews Physics*, 1(4):249–263, 2019.
- [6] Linhong Deng, Xavier Trepat, James P Butler, Emil Millet, Kathleen G Morgan, David A Weitz, and Jeffrey J Fredberg. Fast and slow dynamics of the cytoskeleton. *Nature materials*, 5(8):636–640, 2006.
- [7] Vikram S Deshpande, Robert M McMeeking, and Anthony G Evans. A model for the contractility of the cytoskeleton including the effects of stress-fibre formation and dissociation. *Proceedings of the Royal Society A: Mathematical, Physical and Engineering Sciences*, 463(2079):787–815, 2007.
- [8] Margaret L Gardel, Jennifer Hyunjong Shin, FC MacKintosh, L Mahadevan, Paul Matsudaira, and David A Weitz. Elastic behavior of cross-linked and bundled actin networks. Science, 304(5675):1301–1305, 2004.
- [9] T Christian Gasser, Ray W Ogden, and Gerhard A Holzapfel. Hyperelastic modelling of arterial layers with distributed collagen fibre orientations. *Journal of the royal society interface*, 3(6):15–35, 2006.
- [10] Melville S Green and Arthur V Tobolsky. A new approach to the theory of relaxing polymeric media. The Journal of chemical physics, 14(2):80–92, 1946.
- [11] Albert K Harris, Patricia Wild, and David Stopak. Silicone rubber substrata: a new wrinkle in the study of cell locomotion. Science, 208(4440):177–179, 1980.
- [12] Gerhard A Holzapfel, T Christian Gasser, and Michael Stadler. A structural model for the viscoelastic behavior of arterial walls: continuum formulation and finite element analysis. European Journal of Mechanics-A/Solids, 21(3):441–463, 2002.
- [13] Gerhard A Holzapfel, Thomas C Gasser, and Ray W Ogden. A new constitutive framework for arterial wall mechanics and a comparative study of material models. *Journal of elasticity and the physical science of solids*, 61:1–48, 2000.
- [14] Chung-Yuen Hui, Fan Cui, Alan Zehnder, and Franck J Vernerey. Physically motivated models of polymer networks with dynamic cross-links: comparative study and future outlook. *Proceedings of the Royal Society A*, 477(2255):20210608, 2021
- [15] Chung-Yuen Hui and Rong Long. A constitutive model for the large deformation of a self-healing gel. Soft Matter, 8(31):8209–8216, 2012.

- [16] Ellen Kuhl, Krishna Garikipati, Ellen M Arruda, and Karl Grosh. Remodeling of biological tissue: mechanically induced reorientation of a transversely isotropic chain network. *Journal of the Mechanics and Physics of Solids*, 53(7):1552–1573, 2005.
- [17] Samuel Lamont and Franck J Vernerey. A transient microsphere model for nonlinear viscoelasticity in dynamic polymer networks. Journal of Applied Mechanics, 89(1):011009, 2022.
- [18] Samuel C Lamont, Jason Mulderrig, Nikolaos Bouklas, and Franck J Vernerey. Rate-dependent damage mechanics of polymer networks with reversible bonds. *Macromolecules*, 54(23):10801–10813, 2021.
- [19] Andreas Menzel, Magnus Harrysson, and Matti Ristinmaa. Towards an orientation-distribution-based multi-scale approach for remodelling biological tissues. Computer methods in biomechanics and biomedical engineering, 11(5):505-524, 2008.
- [20] Brian Moran, M Ortiz, and CF1040734 Shih. Formulation of implicit finite element methods for multiplicative finite deformation plasticity. *International Journal for Numerical Methods in Engineering*, 29(3):483–514, 1990.
- [21] Sungmin Nam, Kenneth H Hu, Manish J Butte, and Ovijit Chaudhuri. Strain-enhanced stress relaxation impacts nonlinear elasticity in collagen gels. *Proceedings of the National Academy of Sciences*, 113(20):5492–5497, 2016.
- [22] TD Nguyen, RE Jones, and BL Boyce. Modeling the anisotropic finite-deformation viscoelastic behavior of soft fiber-reinforced composites. *International Journal of Solids and Structures*, 44(25-26):8366-8389, 2007.
- [23] PR Onck, T Koeman, T Van Dillen, and Erik van der Giessen. Alternative explanation of stiffening in cross-linked semiflexible networks. Physical review letters, 95(17):178102, 2005.
- [24] Danielle R Scheff, Steven A Redford, Chatipat Lorpaiboon, Sayantan Majumdar, Aaron R Dinner, and Margaret L Gardel. Actin filament alignment causes mechanical hysteresis in cross-linked networks. Soft Matter, 17(22):5499–5507, 2021.
- [25] David W Speicher and Vincent T Marchesi. Erythrocyte spectrin is comprised of many homologous triple helical segments. Nature, 311(5982):177–180, 1984.
- [26] Shankar Lalitha Sridhar and Franck J Vernerey. Mechanics of transiently cross-linked nematic networks. Journal of the Mechanics and Physics of Solids, 141:104021, 2020.
- [27] Cornelis Storm, Jennifer J Pastore, Fred C MacKintosh, Tom C Lubensky, and Paul A Janmey. Nonlinear elasticity in biological gels. Nature, 435(7039):191–194, 2005.
- [28] R Tharmann, Mireille MAE Claessens, and Andreas R Bausch. Viscoelasticity of isotropically cross-linked actin networks. Physical review letters, 98(8):088103, 2007.
- [29] David Vader, Alexandre Kabla, David Weitz, and Lakshminarayana Mahadevan. Strain-induced alignment in collagen gels. PloS one, 4(6):e5902, 2009.
- [30] Franck J Vernerey. Transient response of nonlinear polymer networks: A kinetic theory. Journal of the Mechanics and Physics of Solids, 115:230–247, 2018.
- [31] Franck J Vernerey. Mechanics of transient semi-flexible networks: Soft-elasticity, stress relaxation and remodeling. *Journal of the Mechanics and Physics of Solids*, 160:104776, 2022.
- [32] Franck J Vernerey and Mehdi Farsad. A constrained mixture approach to mechano-sensing and force generation in contractile cells. *Journal of the mechanical behavior of biomedical materials*, 4(8):1683–1699, 2011.
- [33] Franck J Vernerey, Shankar Lalitha Sridhar, Archish Muralidharan, and Stephanie J Bryant. Mechanics of 3d cell-hydrogel interactions: Experiments, models, and mechanisms. *Chemical Reviews*, 121(18):11085-11148, 2021.
- [34] Franck J Vernerey and Samuel Lamont. Transient mechanics of slide-ring networks: A continuum model. Journal of the Mechanics and Physics of Solids, 146:104212, 2021.
- [35] Franck J Vernerey, Rong Long, and Roberto Brighenti. A statistically-based continuum theory for polymers with transient networks. Journal of the Mechanics and Physics of Solids, 107:1–20, 2017.
- [36] Robert J Wagner, Ethan Hobbs, and Franck J Vernerey. A network model of transient polymers: exploring the micromechanics of nonlinear viscoelasticity. Soft Matter, 17(38):8742–8757, 2021.
- [37] Kuan Wang, J Frederick Ash, and SJ Singer. Filamin, a new high-molecular-weight protein found in smooth muscle and non-muscle cells. Proceedings of the National Academy of Sciences, 72(11):4483–4486, 1975.
- [38] Mark Warner and Eugene Michael Terentjev. Liquid crystal elastomers, volume 120. Oxford university press, 2007.